Original Research Communication

Running head: MSC-therapy protects irradiated lung tissue

Therapy with multipotent mesenchymal stromal cells protects lungs from radiation-induced injury and reduces the risk of lung metastasis

Diana Klein[1], Alexandra Schmetter[1], Roze Imsak[1], Florian Wirsdörfer[1], Kristian Unger[2], Holger Jastrow[3], Martin Stuschke[4], Verena Jendrossek[1]

[1]Institute of Cell Biology (Cancer Research), University of Duisburg-Essen, University Hospital, 45122 Essen, North Rhine-Westphalia, Germany.

[2]Research Unit Radiation Cytogenetics, Helmholtz Center Munich, German Research Center for Environmental Health GmbH, 85764 Neuherberg, Bavaria, Germany.

[3]Institute of Anatomy, University of Duisburg-Essen, University Hospital, Essen, Germany.

[4]Department of Radiotherapy, University of Duisburg-Essen, University Hospital, 45122 Essen, North Rhine-Westphalia, Germany.

Correspondence to

Prof. Dr. Verena Jendrossek

Institute of Cell Biology (Cancer Research)

University Hospital Essen, University of Duisburg-Essen

Virchowstr. 173, Ger-45147 Essen

Tel: +49-201-723 3380; Fax: +49-201-723 5904

E-mail: verena.jendrossek@uni-due.de

Word count (excluding References and Figure legends): 7009
Reference number: 75
Number of grey scale illustrations for print version: 8 (Figure 1- 8)
Number of color illustrations for online version: 8 (Figure 1-8)

Abstract

Aims

Previous thorax irradiation promotes metastatic spread of tumor cells to the lung. We hypothesized that vascular damage facilitates lung metastasis after thorax irradiation and that therapeutically applied multipotent mesenchymal stromal cells (MSCs) with reported repair activity may prevent these adverse effects of ionizing radiation by protecting lung endothelia from radiation-induced damage.

Results

Previous whole thorax irradiation (WTI) with 15Gy significantly enhanced seeding and metastatic growth of tumor cells in the lung. WTI was further associated with endothelial cell damage, senescence of lung epithelial cells and up-regulation of invasion- and inflammation-promoting soluble factors, e.g. endothelial matrix metalloproteinase 2 (Mmp2), its activator Mmp14, the co-factor tissue inhibitor of metalloproteinases 2 (Timp2), chemokine (C-C motif) ligand 2 (Ccl2), and urokinase-type plasminogen activator (Plau/uPA), and recruitment of CD11b+CD11c- myelomonocytic cells. Inhibition of Mmp2 counteracted radiation-induced vascular dysfunction without preventing increased metastasis. In contrast, therapy with bone marrow or aorta-derived MSCs within two weeks post-irradiation antagonized radiation-induced damage to resident cells as well as the resulting secretome-changes and abrogated the metastasis-promoting effects of WTI.

Innovation

Therapy with MSCs protects lungs from radiation-induced injury and reduces the risk of lung metastasis. MSC-mediated inhibition of Mmp2 mediates their protective effects at the vasculature. Further local and systemic effects such as inhibition of radiation-induced senescence of bronchial epithelial cells and associated secretion of immunomodulatory factors may participate in the inhibitory effect of MSCs on lung metastasis.

Conclusion

MSC-therapy is a promising strategy to prevent radiation-induced lung injury and the resulting increased risk of metastasis.

Introduction

Radiotherapy (RT) plays a key role in cancer treatment and is highly effective in reducing tumor growth. The ultimate goal of radiation therapy is to reduce or eliminate tumor burden while sparing normal tissues from long-term injury. However, local recurrence of primary tumors and distant metastasis are the leading causes of death in many cancer patients (18). Herein the high intrinsic sensitivity of normal tissues to ionizing radiation (IR) often precludes the application of curative radiation doses (23,60). As an example, thorax irradiation induces tissue inflammation (pneumonitis) and fibrosis as dose-limiting side effects with a lethality of up to 15% (27). Moreover, some recent studies raise the possibility that thorax irradiation not only triggers efficient eradication of cancer cells but also facilitates seeding of surviving tumor cells to the irradiated lung tissue and thus tumor recurrence under certain conditions (11,29,56). However, the underlying mechanisms of radiation-induced adverse late effects are still not well understood and no causative radioprotective treatment is available to date.

Others and we showed in preclinical studies that radiation-induced normal tissue toxicity is closely linked to vascular endothelial cell damage and dysfunction of the blood-air-barrier (9,20,22,71). Moreover, investigations in murine models suggest that radiation-induced endothelial cell damage favors the transmigration of tumor cells through the endothelium - which is a critical step in the metastatic cascade- resulting in increased formation of micrometastasis (5,7,29). Dysregulated proteolysis has been implicated in tumor invasion and metastasis by promoting tumor cell transendothelial migration. In particular matrix metalloproteinases (Mmps) have previously been shown to degrade the extracellular matrix and the basement membrane in the process of metastasis (49). Interestingly invasive breast cancer cells foster endothelial barrier dysfunction by the activation of endothelial Mmp2 production and thereby facilitate tumor cell extravasation through lung microvascular endothelial cells (36,54). We therefore speculated that the primary damage and functional impairment of the endothelial cell (EC) facilitates the formation of micrometastasis in the irradiated lung tissue.

Further investigations including own previous work revealed that IR induces complex immune changes such as secretion of cytokines/chemokines and recruitment of cells from the innate and adaptive immune system (11,70). Interestingly, tumors grown in previously irradiated tissues also recruit large numbers of bone marrow (BM)-derived CD11b+ myeloid cells to support their growth (1,70). However, the role of immune cells infiltrating irradiated tissues for treatment outcome is still controversial as they can either enhance the antitumor effects of RT or provide paracrine signals that facilitate tumor cell survival and growth, including the formation of tumor blood vessels (1,3,44,69).

Up to now, the mechanisms driving immune cell recruitment or tumor cell recruitment to irradiated tissues are still unclear. Herein, a biological process that can be initiated in various cells in response to diverse stressors including IR and has the potential to generate paracrine signals affecting the recruitment of tumor cells and immune cells is cellular senescence. Senescence is aimed to remove irreparable damaged and therefore potentially harmful cells from the proliferative pool. Though senescent cells do not proliferate they acquire a particular phenotype characterized by complex gene expression changes and increased expression of diverse secreted proteins termed “senescence-associated secretory pattern” (SASP).

The SASP includes inflammatory cytokines, growth factors, and proteases with potential immune modulatory function and some of the SASP proteins even have a suspected tumor-promoting effect (8,14,15,43). It has been demonstrated that single SASP factors regulate key processes that facilitate tumor progression and metastasis including proliferation, senescence, angiogenesis, epithelial mesenchymal transition and immune evasion (2,53,55). However, the involvement of senescence in radiation-induced adverse effects has not yet been investigated.

Stem cell therapy is a promising option for the prevention or treatment of radiation-induced normal tissue injury as they can promote survival and repair of damaged cells (16). Moreover, transplantation of bone marrow-derived mesenchymal stem cells, also referred as multipotent mesenchymal stromal cells (MSCs) has established itself as a potential strategy

for the treatment of lung diseases (46,63). However, there is a lack of preclinical and clinical studies of stem cell therapy for radiation-induced adverse effects in the lung (46,58) and there are only few ongoing clinical trials with MSCs in chronic lung disease including their therapeutic applications in patients with idiopathic pulmonary fibrosis (61,62). We hypothesized that therapeutic application of MSCs may be suited to promote repair of radiation-induced damage to resident lung cells, particularly vascular endothelial cells, thereby reducing settlement of tumor cells to previously irradiated lung tissues. A common source of MSCs is the BM (51). However, the procedure to collect BM-derived MSCs is very invasive and only 0.01 to 0.001 percent of mononuclear cells in the BM are MSCs so that other, more accessible sources would represent good alternatives. In addition, cord blood, placenta, blood, fetal liver, and even adipose tissue can be used to obtain human MSCs (26,34,37,75). Above all, cord blood and peripheral blood could be good and easily accessible sources (30,31). However, the percentage of hMSCs in peripheral blood is very low. Therefore, the donor must be stimulated with GM-CSF to increase this percentage by a washout of MSCs from the BM, but this is very distressing and stressful for the patient. We showed in previous studies that nestin-positive multipotent MSCs reside in the wall of adult blood vessels and may serve as source for tissue-specific MSCs (vascular wall-resident MSCs, VW-MSCs). In patho-physiological conditions, e.g. the neovascularization of tumors, these VW-MSCs are involved in the stabilization of newly formed vessels and exhibit classical behavior of MSCs *in vitro* (40,41). In order to obtain sufficient material for experimental studies, these cells can be isolated directly *ex vivo* from the largest blood vessel of the murine system, the aorta, and cultured upon immunomagnetic separation using the Stem Cell Antigen 1 (Sca1). For human use, VW-MSCs can be isolated from small vessel pieces (excess material) obtained during surgery (e.g. vena saphena or arteria radialis).

Importantly, tissue-specific stem cells differentiate mainly to the tissue-type from which they derive, indicating that there is a certain code ("priming") within the cells as determined by the tissue of origin. Beside the relatively simple extraction of these cells for autologous

transplantation this might be a particular advantage for the therapeutic application of VW-MSCs for improving vascular function or preventing vascular damage. We therefore hypothesized that therapeutic application of VW-MSC might be particularly well suited for for the radioprotection of endothelial cells in a murine model of radiation-induced lung injury.

Here we used MSCs isolated either from the BM or from the aorta (Ao) to investigate their potential to counteract lung injury and the resulting microenvironmental changes in response to whole thorax irradiation (WTI) and explore the underlying mechanisms in a murine model. We show that thorax irradiation induces vascular damage, senescence of bronchial epithelial cells and secretion of SASP factors with suspected tumor-promoting potential. These changes were associated with an enhanced metastasis of intravenously injected tumor cells or subcutaneously growing tumors to previously irradiated lungs. Adoptive transfer of MSCs normalized vascular dysfunction through inhibition of endothelial Mmp2, reversed epithelial cell senescence and certain aspects of the associated SASP, and reduced the risk of lung metastasis. We speculate that MSC-mediated protection of the lung tissue from the damaging effect of IR precludes the initiation of a tumor-promoting signaling network between damaged resident cells, recruited immune cells and tumor cells that supports invasion and growth of invading tumor cells.

Results

Impaired vascular function after WTI is accompanied by increased tumor cell extravasation and metastasis in experimental models

To investigate a suggested general metastasis-promoting effect of ionizing radiation we studied seeding and growth of intravenously injected tumor cells in previously irradiated lung tissue using two different murine cells lines. For this, C57BL/6 mice and BALB/c mice were irradiated with 15Gy WTI and syngeneic tumor cells (B16F10 melanoma cells for C57BL/6 mice and TS/A mammary adenocarcinoma cells for BALB/c mice) were injected into tail vein at 21 days post-irradiation (Fig. 1A,B). Micrometastasis formation and subsequent formation of macrometastasis was significantly increased in lungs 14 days after tumor cell injection in both mouse strains [(C57BL/6/ 15Gy: 26.5 per lung cross section ± 4.6 [standard error of the mean, SEM], n=10; 0Gy: 12.2 ± 4.1, n = 13; $P<0.05$; BALB/c 15Gy: 24.7 ± 3.5, n = 11; 0Gy: 10.6 ± 2.9, n = 9; $P<0.05$ as analyzed by two-way ANOVA followed by post-hoc Bonferroni test: F-factors 0.00297 (interaction), 11.64 (column factor, cf / Gy), 0.2247 (row factor, rf / mouse strain)]. Though tail-vein injection of cancer cells is a well-established model of experimental metastasis (66) we next aimed to exclude that the observed effects may be artifacts of injecting large tumor cell numbers into the circulation. Therefore we performed additional experiments measuring metastasis formation of subcutaneously growing C57Bl/6 xenograft flank tumors. For this, C57BL/6 mice received a lethal total body irradiation (TBI) with a splitting dose of 7+3Gy followed by bone BM reconstitution and subcutaneous implantation of B16F10 tumor cells into the flank at 4 - 6 weeks post-irradiation. Two or 28 days later tumor cell extravasation (here designated as micrometastasis) and subsequent growth of macrometastasis were quantified in whole lung sections (Fig. 1C). These data revealed that metastatic spread to previously irradiated lungs is also increased in mice bearing subcutaneously growing tumors [(28d/ 10Gy: 8.2 ± 1.3, n = 22; 28d/ 0Gy: 14.1 ± 1.0, n = 11; $P<0.01$; 2d/ 15Gy: 8.7 ± 2.5, n = 18; 2d/ 0Gy: 1.2 ± 0.4, n = 11; $P<0.05$ as analyzed by two-way ANOVA followed by post-hoc Bonferroni test: F-factors 1.026 (interaction), 12.17 (cf / Gy), 0.5355 (rf / days)].

Because the observed effects in the different models were rather similar, all subsequent experiments were only performed in the B16F10 melanoma model using C57BL/6 mice. Next we aimed to gain more detailed insight into the effects of WTI on the vascular compartment. An intensive morphological analysis of the lung tissue at 21 days after WTI corroborated the suggested link between the increased radiation-induced seeding of circulating tumor cells and a functional impairment of lung endothelial cells (EC) (Fig. 2A). Indeed, arterial EC showed numerous vacuoles, partially degraded mitochondria (Fig. 2A2,A3), and a defective and irregular basement membrane (bMem) lining arterial EC (Fig. 2 A4, arrow heads) at d21 post-irradiation, though EC junctions were not affected. The regular arrangement of EC junctions was further analysed by Western blot analysis of protein cell lysates obtained from whole mouse lung (Fig. 2B). The total amount of VE-cadherin (VE-Cad) as well as its low phosphorylation status and the proper association with beta-catenin was not altered after WTI. Real Time RT-PCR quantification of *VE-Cad* mRNA levels in whole lung RNA isolates further confirmed no alterations of *VE-Cad* expressions after WTI (Fig. 2C). Immunocolocalization of VE-Cad and endothelial CD31 (PECAM1) expression confirmed cell surface localization of VE-Cad in lung EC and a regular arrangement after WTI (Fig. 2D). These results suggest that IR-induced endothelial cell damage facilitates the transmigration of tumor cells through the endothelium - a critical step in the metastatic cascade.

MSC-therapy improves vascular dysfunction and reduces lung metastasis to previously irradiated lungs

Next, we explored a novel therapeutic strategy based on therapeutic application of MSCs to limit the radiation-induced vascular dysfunction and the associated risk of increased growth of metastatic tumor cells in previously irradiated lungs. EGFP-tagged MSCs were routinely isolated and cultured from aorta (Ao) of EGFP-Nagy mice and from the BM. C57BL/6 mice received 15Gy WTI followed by intravenously transplantation of single cell suspensions of cultured EGFP positive (EGFP(+)) MSCs into the tail vein at 24 hours or 14 days after irradiation (Fig. 3). RT-induced vascular dysfunction resulted in increased albumin leakage (Fig. 3A: difference in mean mg Evans blue dye (EBD) per mg lung tissue = 0.13; control

irradiated mice = 0.06, n= 5 and WTI mice = 0.19, n = 5, P<0.05 (95% confidence interval [CI] = 0.01 to 0.24). IR-induced impairment of EC function as determined by EBD extravasation was restored 21 days after irradiation in MSC-treated animals at both, 24 hours and 14 days after RT, independently from the origin of the applied MSCs (mean EBD extravasation = -0.13 of WTI and BM24h, n = 5, 95%CI =,-0.24 to -0.002, P<0.05; Ao24h = -0.10, 95% CI = -0.2 to 0.006, P =0.06; BM14d = -0.14, 95% CI = -0.26 to -0.02, P<0.05; Ao14d = -0.10, 95% CI=-0.24 to 0.04, P=0.15). Electron microscopy of lung blood vessels demonstrated a regular vessel structure as well as restored regular EC morphology in the lungs of MSC-treated animals (Fig. 3B). Immunofluorescent analysis of EGFP expression in isolated lung sections revealed that only a few, preferably single donor cells can be detected in lung sections, indicating that nearly no therapeutically applied EGFP(+) MSCs homed to the injured lung tissue 21 days after WTI while circulating EGFP(+) MSCs could still be detected in peripheral blood several weeks after transplantation (Fig. 3C). Quantification of lung metastasis formation (Fig. 3D) demonstrated that application of MSC derived from BM or Ao within 24 hours after irradiation [15Gy: 36.9 metastasis per lung cross section ± 4.80 (SEM), n = 33; 0Gy: 7.4 ± 1.9, n=10, P<0.001; 0GyAo24h: 2.4 ± 1.3, n = 8, P<0.001; 15GyBM24h: 13.0 ± 5.8, n = 9, P<0.05; Ao24h: 11.3 ± 3.9, n = 7, P<0.05] or 14 days later [BM14d: 10.3 ± 4.1, n = 13, P<0.001; Ao14d: 11.4 ± 6.1, n = 9, P<0.05 as analyzed by two-way ANOVA followed by post-hoc Bonferroni test: F-factors 13.297 (interaction), 11.44 (cf / Gy), 7.248 (rf / treatment)] significantly reduced seeding of circulating tumor cells and subsequent metastasis formation. A similar tendency to a pronounced but not significantly reduced metastasis formation was also detected in MSC-treated animals after sham irradiation. These results demonstrate that therapeutic application of MSCs has a high potential to counteract seeding and growth of circulating tumor cells in previously irradiated lungs. To exclude that MSC-therapy has itself a metastasis-promoting effect on established tumors, untreated C57BL/6 mice were first intravenously injected with B16F10 cells into the tail vein and metastasis formation and growth was allowed for 14 days (Fig. 3E). Thereafter animals received a 15Gy WTI without or with additional adoptive transfer of cultured MSCs (0.5*10(6) cells) derived from the aorta 24h after irradiation (15GyAo24h). Quantification of

lung metastasis at 3 weeks after MSC-therapy revealed that MSC-therapy did not increase the number or size of established lung metastasis. These results indicate that MSC-therapy reduces the risk of lung metastasis in irradiated lungs without promoting growth of established metastatic lesions.

MSC treatment reduces radiation-induced endothelial Mmp2 expression thereby normalizing vascular function

Invasion and metastasis of tumor cells requires proteolytic activity (e.g. Mmps) in order to degrade components of the extracellular matrix thereby facilitating tumor cell migration as well as metastatic dissemination of malignant cells. Therefore, we analyzed expression levels of *Mmp2* as well as of its co-factors *Mmp14* and *Timp2* in more detail in irradiated lung tissue (Fig. 4). Real-Time RT-PCR quantification of these metastasis associated genes revealed a significant up-regulation of the *Mmp2-Mmp14-Timp2* axis in the lungs of WTI animals after WTI [Fig. 4A; P values as indicated: *P<0.05, **P<0.01, ***P<0.001 as analyzed by two-way ANOVA followed by post-hoc Bonferroni test: F-factors 2.311 (interaction), 9.589 (cf / Gy and treatment), 5.721 (rf / genes)]. Of note, the mRNA levels of these enzymes were almost reduced to normal levels when animals were treated with MSCs from BM from Ao within 24h after irradiation (Fig. 4A). Increased radiation-induced Mmp2 expression was further confirmed on protein level as shown by using Western blot analysis in whole protein lysates and in paraffin sections using immunohistochemistry (Fig. 4B). Increased amounts of Mmp2 protein levels were confined to arterial blood vessels of lungs compared after WTI; notably, Mmp2 levels were reduced in lungs of animals treated with IR plus subsequent MSC-therapy (Fig. 4C). To confirm the endothelial origin of Mmp2, mouse lung endothelial cells (MLEC) were purified and irradiated *in vitro*. Interestingly, IR of cultured MLEC induced an up-regulation of Mmp2 and an increased secretion of Mmp2 to the medium (not shown). These results suggest that endothelial Mmp2 contributes to radiation-induced EC damage and can be targeted by MSC-therapy.

To gain insight into the role of Mmp2 in the adverse effects of RT to the lung we examined potential protective effects of a specific Mmp2 inhibitor in our experimental model. For this

C57BL/6 mice received repeated intra-peritoneal injections of the selective Mmp2 inhibitor ARP100 (15µg/g bodyweight) twice a week for 3 weeks after WTI (Fig. 5). As shown in Fig. 5A and 5B, ARP100-treatment normalized RT-induced BSA-extravasation at day 21 post-irradiation (15Gy: 6.8 ± 2.9 µg BSA/ g total lung protein, means ± SEM, n = 4; 15Gy/ ARP100: 0.5 ± 0.5 µg BSA/ g total lung protein, means ± SEM, n=6, $P<0.05$). Moreover, Mmp2 inhibitor treatment restored regular EC morphology and vessel structures in the lungs of WTI mice (Fig. 5C). However, Mmp2 inhibition was not sufficient to significantly reduce colonization of previously irradiated lungs by circulating tumor cells [Fig. 5D,E; difference in mean counts (ME) of sham irradiated mice (n=10) and WTI mice (n=15) = 35.7 (95% CI=22.5 to 48.8), $P<0.001$ (comparison to 15Gy) as determined by one-way ANOVA followed by post-hoc Bonferroni test; ME of WTI mice and Mmp2 inhibitor-treated WTI mice (n = 6): not significant]. These data indicated that MSC inhibition of vascular dysfunction involves down-regulation of endothelial Mmp2 in irradiated lung tissue.

MSC-therapy counteracts radiation-induced senescence of resident epithelial cells and recruited immune cells

As Mmp2 is not only linked with vascular dysfunction and tumor cell invasion but also a well-known factor associated with senescence we next investigated whether WTI might induce cellular senescence (Fig. 6). Therefore senescence-associated beta-galactosidase (SAbetagal) activity was assessed in frozen lung tissue sections at 21 days post-irradiation in lung tissue from control and WTI animals with or without additional MSC-therapy. Interestingly increased SAbetagal activity was detected in bronchial-alveolar epithelial cell in lungs after WTI when compared to lung sections from control animals (Fig. 6A). In lungs of MSC-treated animals SAbetagal activity showed a staining pattern comparable to lung sections from control animals. Apart from epithelial cells single infiltrating cells were also SAbetagal-positive, suggesting IR-induced immune-senescence. Indeed, co-immuno-stainings with CD45 antibody identified these cells to be leukocytes (Fig. 6A upper right panel). WTI induced senescence induction was further confirmed on mRNA level by Real-Time RT-PCR quantification of the cellular senescence mediator gene *cyclin-dependent*

kinase inhibitor 1 (*Cdkn1a, p21*) as well as on protein level (Fig. 6B,C). Notably, Cdkn1a expression levels were significantly decreased in lungs of irradiated animals treated with MSC. To gain insight into the resulting effects of MSC-therapy on immune cell recruitment, infiltrating CD45+ leukocytes were quantified by counting numbers of CD45-immunoreactive structures in frozen sections of lung tissue from control and irradiated animals with or without additional MSC-therapy. The numbers of infiltrating CD45+ cells were increased in tissue sections of irradiated animals at 21d after WTI and their numbers were significantly reduced upon MSC-therapy [Fig. 6D; P values as indicated: *P<0.05, as analyzed by two-way ANOVA followed by post-hoc Bonferroni test: F-factors 0.5583 (interaction), 14.32 (cf / Gy), 3.645 (rf / treatment)]. These findings indicated that WTI-induces senescence of bronchial-alveolar epithelial cells as well as leukocyte infiltration and that both effects are antagonized by MSC treatment.

MSC-therapy counteracts certain aspects of the secretome of irradiated lungs and the recruitment of myeloid cells with reported tumor-promoting potential

Since SASP factors like the *chemokine (C-C motif) ligand 2* (*Ccl2*) and *urokinase-type plasminogen activator* (*Plau/uPA*) are known to be involved in both immune regulation and metastasis we next examined whether WTI would increase the levels of these factors in the lung tissue. Quantification of *Plau/uPA* and *Ccl2 mRNA* expression levels showed increased *Plau/uPA* and *Ccl2* mRNA expression levels in total lung RNA isolates of irradiated lungs when compared to lung tissue from sham-irradiated control mice (Fig. 7A). Of note, adoptive transfer of MSC normalized the expression levels of *Ccl2* and to a lesser extent of *Plau* in lungs of irradiated animals. A similar tendency to decreased expression levels of *Ccl2* and *Plau* mRNA was also detected in MSC-treated animals sham controls compared to sham controls without MSC treatment [Fig. 7A; P values as indicated: *P<0.05, ***P<0.001 as analyzed by two-way ANOVA followed by post-hoc Bonferroni test: F-factors 2.560 (interaction), 4.422 (cf / Gy and treatment), 1.990 (rf / gene)]. Immunohistochemistry analysis of Ccl2 and Plau/uPA proteins further revealed that radiation-induced Ccl2 and Plau/uPA expression confined to the bronchial-alveolar epithelial cells in irradiated lungs (Fig. 7B).

Notably, these levels were reduced in lungs of animals treated with IR plus subsequent MSC-therapy.

Since Ccl2 has been linked to immune modulation we further investigated whether RT-induced alterations in the lung secretome may result in altered recruitment of myeloid cells. For this, we analysed the composition of the myeloid cell compartment by FACS analysis of cell extracts generated from freshly isolated lung tissue. Interestingly, the percentage of CD11b+CD11c- myeloid cells (monocytes/granulocytes) from CD45+ leukocytes, particularly of Ly6C+ (myelomonocytic cells), was significantly increased after WTI whereas the percentage of CD11bintCD11c+ cells (alveolar macrophages) was decreased when compared to sham controls (Fig. 7C,D; P value as indicated: $P \leq 0.05$, $^{**}P \leq 0.01$, $^{***}P \leq 0.001$ as analyzed by two-way ANOVA followed by post-hoc Bonferroni test [for **C**: F-factors 0.48 (interaction), 11.77 (cf / Gy), 1.268 (rf / treatment); for **D**: F-factors 9.026 (interaction), 1.025 (cf / Gy), 327.5(rf / marker)]. Even more important, MSC-therapy antagonized infiltration of Ly6C+ and CD11b+CD11c- myeloid cells with high efficiency (Fig. 7C,D). These data suggest that abrogation of certain aspects of the secretome of irradiated resident lung cells and the resulting immune deviation may participate in MSC-mediated protection from RT-induced lung injury and metastasis.

Discussion

Here we demonstrate for the first time that MSC-therapy has the potential to protect the highly radiosensitive lung tissue from radiation-induced damage to vascular structures and the associated increase in lung metastasis in experimental murine models. Moreover, we identified enhanced senescence of lung epithelial cells, secretion of the SASP factors Mmp2, Plau/uPA and Ccl2 as well as increased recruitment of CD11b+CD11c- myelomonocytic cells as novel factors participating in the response of the normal lung tissue to ionizing radiation. Importantly, we identified inhibition of Mmp2 as the mechanism underlying MSC-mediated normalization of vascular dysfunction. The observation that Mmp2 inhibition did not significantly reduce increased lung metastasis indicates that further cellular or paracrine effects of MSC participate in their protective effects against lung metastasis. These may include protection of bronchial epithelial cells from radiation-induced senescence, suppression of tumor-promoting SASP-factors and/or modulation of radiation-induced lung inflammation.

Our data corroborate earlier reports about a delayed disturbance of endothelial barrier function in the lung tissue at 21 days post-irradiation (9) and the resulting increase in transmigration of tumor cells through the endothelium (5,7,29). In our hands the pro-metastatic effect of RT was observed for two distinct cell lines (B16F10 melanoma and TS/adenocarcinoma) injected into the tail vein of the two distinct respective syngeneic mouse strains (C57BL/6 and BALB/c). Furthermore, the enhancement of tumor cell seeding to previously irradiated lung tissue was observed with tumor cells injected into the tail vein as well as with subcutaneously growing tumors. These observations point to a more general cell line and mouse strain-independent phenomenon presumably initiated by radiation-induced microenvironmental changes.

Though the reason for the formation of micrometastasis in specific organs is still unknown, this process requires adhesion of the tumor cells to the vessel wall, followed by the emigration of the tumor cells into the surrounding tissue (32,52). We show here that radiation-induced tissue damage activates pro-invasive and pro-metastatic signals such as

up-regulation of endothelial *Mmp2* as well as *Mmp14* and *Timp2* suspected to promote the invasion of circulating tumor cells to irradiated lung tissue. However, though administration of a selective Mmp2 inhibitor restored EC morphology and function in the lungs of irradiated mice Mmp2-inhibition was not sufficient to significantly reduce seeding and growth of circulating tumor cells in irradiated lungs. Though we cannot exclude that the inhibition of tumor cell extravasation and subsequent metastatic growth might require higher Mmp2 inhibitor concentrations these findings strongly suggest the contribution of additional mechanisms. Nevertheless, our data demonstrate a role of Mmp2 for radiation-induced vascular dysfunction in the lung and offer novel perspectives for the treatment of lung pathologies associated with radiation-induced EC-damage such as pulmonary arterial hypertension (PAH). Here, a functional impairment or even partial loss of the endothelial cells as a result of selective lung irradiation was detected long before the clinical manifestation of the disease (24).

Interestingly, our further investigations revealed that WTI triggers a pronounced senescence of bronchial epithelial cells. These findings corroborate observations made by by Li and coworkers about the induction of senescence markers in murine brain, lung and liver tissue exposed to a sublethal dose of IR *in vivo* (43). Cellular senescence is a tumor-suppressive mechanism that permanently arrests cells at risk for malignant transformation. However, accumulating evidence shows that senescent cells can have deleterious effects on the tissue microenvironment and may even fuel the development of secondary cancers (14,48). A potential link between cellular senescence and metastasis has recently been established by Shimizu and coworkers who found higher numbers of lung metastasis from intravenously injected K1735M2 melanoma cells in aged compared to young SAMP10 (senescence-accelerated mouse prone 10) mice (55). The authors concluded that aging-associated senescence facilitates metastasis due to the decrease in immune surveillance in the aging microenvironment. Vice-versa oncogene-induced senescence in proliferating breast cancer cells through expression of p95HER2, a 80 to 115 kDa carboxy-terminal and constitutively active fragment of the tyrosine kinase receptor HER2, increased their metastatic potential presumably through the senescence secretome of the cancer cells (2). Thus, the pro-tumor

effects of senescent cells are linked to the senescence-associated secretome, or SASP, which seems to be shaped by the respective stimulus, e.g. ionizing radiation or oncogenic transformation (2,14).

We show here that senescence of bronchial epithelial cells from irradiated mice is associated with increased secretion of further SASP factors such as Ccl2 and Plau/uPA. There is accumulating evidence that senescent cells secrete various pro-inflammatory cytokines and chemokines known to play a vital role in tumor progression and metastasis (42,53,59). As an example, Ccl2 has been associated with poor clinical outcomes in several cancers, including myeloma, breast cancer, and prostate cancer (17). Furthermore, Ccl2-induced recruitment of Ly6C(+) myeloid cells promoted cancer cell metastasis to the lung (64). Myelomonocytic cells were also shown to be essential for the establishment of a premetastatic niche and survival of metastatic cells in mice (25). Vice-versa, Plau/uPA was reported to contribute to cancer cell invasion and metastasis (47). Plau/uPA catalyzes the transformation of plasminogen to plasmin, which degrades extracellular matrix molecules and basement membranes directly or indirectly through activating pro-matrix metalloproteinases (pro-Mmps) thereby facilitating cancer cell invasion and metastasis (65).

From the vast majority of cancer cells that enter the circulatory system, only very few successfully engraft, survive, and proliferate at secondary sites (35,67). Therefore it is tempting to speculate that radiation-induced lung injury including senescence of lung epithelial cells and the resulting increase in secreted factors like Mmp2, Ccl2 and Plau/uPA participate in the generation of a receiving microenvironment (“niche”) that enables seeding, survival and growth of metastatic tumor cells (Fig. 8). However, the functional relevance of specific secreted factors and the resulting immune changes for increased lung metastasis remains to be demonstrated.

Current research efforts are aimed at protecting adjacent tissues in order to minimize the risk of recurrence. It is assumed that adult MSCs may be a valuable therapeutic option for the prevention of lung diseases or the regeneration of diseased lung tissue, because these cells are relatively easily available, have immunomodulatory effects and have the capacity for cell differentiation (6,62), though engraftment in the lung as structural epithelium or endothelium

is not currently considered the mechanism by which BM-MSCs can repair lung tissue (63). Here we investigated the therapeutic potential of MSC derived classically from BM or from aorta to protect the lung tissue from radiation-induced injury and the resulting increase in lung metastasis from circulating tumor cells. We demonstrate that MSCs derived from BM and aorta both efficiently counteract RT-induced vascular damage. The high activity of the aorta-derived MSCs for EC protection might be due to the fact that tissue-specific stem cells mainly support the tissue type from which they originate (21). Several studies have shown that MSCs provide an important contribution to tissue neovascularization by migrating to the site of damage and differentiating to restore damaged cell types (13,68). However, the greatest potential of MSCs in terms of neovascularization is attributed to the trophic effects e.g. to prevent fibrosis and apoptosis, or to promote angiogenesis and arteriogenesis due to the production of cytokines for a paracrine action (33,50,73). A similar observation could be made in the animal model of pulmonary arterial hypertension. Here, the therapeutic use of bone marrow MSCs led to a reduced vascular remodeling and increased expression of VEGF (45). We found here that treatment with an inhibition of Mmp2 mimics the beneficial effect of MSC-therapy on vascular function in irradiated lungs. This implicates that up-regulation of Mmp2 participates in the pathogenesis of radiation-induced vascular dysfunction. Moreover, previous studies have shown that BM-MSCs migrate to injured tissues, communicate with injured parenchyma cells, and function in wound healing through the production of paracrine-soluble cytokines/chemokines and growth factors which modulate the regeneration of the epithelium and endothelium and modulate the activation, proliferation, and downstream effects of inflammatory and immune cells in both the innate and adaptive immune systems (12,63,74). Therefore it is highly likely that the therapeutically applied MSCs exert their beneficial effects in the irradiated lungs by the secretion of multiple paracrine factors or the modulation of the secretory activity of damaged resident cells and/or recruited immune cells that have yet to be identified.

Even more important, we demonstrate here for the first time that therapeutically applied MSCs also prevent the seeding of circulating tumor cells. The inhibitory effect of MSC on lung metastasis was associated with a reduction in RT-induced senescence of bronchial

epithelial cells and expression of SASP factors such as Ccl2. As outlined above, Ccl2 and Plau/uPA may be linked to the recruitment of CD11b+CD11c- myeloid cells to the lung and these cells have reported tumor-promoting activity (Fig. 8). This assumption is supported by the finding that metastatic cancer cells can co-opt chemokine pathways to migrate to distant sites, in particular those chemokines that normally regulate the migration of immune cells (53). Moreover it has been shown in rats that therapeutically applied MSCs can down-regulate inflammatory mediators through paracrine effects and by reducing alveolar cell apoptosis and lung inflammation responses (72). However, the functional relevance of our observations for the mechanisms of MSC-mediated tissue protection needs to be addressed in future studies.

Our data reveal that MSC have a high potential for the development of protective treatment strategies in irradiated patients. First clinical applications of stem cell transplantation indicate a potential of these cells in bone regeneration as well as immunosuppressive effects after allogeneic stem cell transplantation. Isolated from the bone marrow MSCs are already used in the clinic in patients with dilated myopathy, cartilage disorders, stroke, and autoimmune diseases (4,10,57). In line with these findings, we show here that intravenously applied MSCs lingered in the circulation and only single cells homed to irradiated lung tissue when cells where applied in the early phase of irradiation. Fortunately, no adverse effects on progression of lung pathology were found (not shown).

In summary, the high radiosensitivity of lung resident cells plays a crucial role for radiation-induced lung disease and the metastatic colonization of previously irradiated lungs by intravenously injected tumor cells or subcutaneously growing tumors. Adoptive transfer of MSCs counteracts radiation-induced vascular damage, bronchial-epithelial senescence, and metastasis of circulating tumor cells to the irradiated lungs. We speculate that down-regulation of radiation-induced expression of endothelial Mmp2 and of the SASP factors Ccl2 and Plau/uPA as well as a reduced infiltration of metastasis-promoting myeloid cells are involved in the protective action of MSC. However, the role of specific SASP factors for the niche-promoting effects of RT in the suspected network between damaged cells, immune cells and invading tumors cells remain to be demonstrated. These investigations will be

performed in further studies using mouse models deficient for single SASP factors or the respective specific inhibitors. Our results are of direct clinical relevance, since they contribute to an improved understanding of the mechanisms of the dose-limiting side effects of radiotherapy. This is a necessary step in the development of protective treatment strategies.

Innovation

The high intrinsic radiosensitivity of the lung tissue precludes the use of curative radiation doses and fosters a therapeutic failure by local tumor recurrence and metastasis. Here we demonstrate that therapy with BM-derived or vascular wall-derived MSCs protect the lung tissue from radiation-induced vascular dysfunction through inhibition of Mmp2 and antagonizes increased metastasis of circulating tumor cells to previously irradiated lungs. MSC-therapy also reversed radiation-induced senescence of epithelial cells and suppressed associated secretion of SASP factors and immune changes. Thus, MSC-therapy is a promising strategy to prevent radiation-induced local and systemic effects with suggested tumor-promoting potential.

Materials and Methods

Tumor cells and mouse models

B16F10 (ATCC® CRL-6475; ATCC, Manassas, VA) mouse melanoma and TS/A murine mammary adenocarcinoma cells were cultured in DMEM/10% FCS (5% CO2 at 37°C). The TS/A cell line is a moderately differentiated and immunogenic mammary adenocarcinoma of spontaneous BABL/c origin (28). Wild type C57BL/6 and BABL/c mice received 15 Gray of WTI in a single dose of a Cobalt 60 source (^{60}Co γ-rays at 0.5 Gy/min) as previously described (69). Single cell suspensions of cultured MSCs (0.5*10(6) cells) were intravenously transplanted into the tail vein of WTI mice 24 hours or 14 days after irradiation or in sham irradiated (0Gy) control animals. Seeding of circulating tumor cells into the lungs was initiated 21 days after irradiation. Preliminary tests for cell numbers were performed in order to determine the optimal tumor cell number for intravenous injection and resulting quantifiable metastasis. Consequently, 1*10(6) B16F10 cells or TS/A cells were intravenously transplanted via the tail vein in the subsequent experiments. Fourteen days after tumor cell injection animals were sacrificed and lungs were isolated subjected for IHC, RNA or protein isolation.

Additionally, we examined seeding of lung metastases in mice exposed to total body irradiation (TBI) and subsequent implantation of subcutaneous tumors (40). In brief, C57BL/6 mice were lethally irradiated with a split dose (7+3 Gy) of a X-ray source (3Gy/min) and were intravenously transplanted with 2x10^6 unfractioned murine EGFP-expressing BM cells from C57BL/6-Tg(CAG-EGFP)1Osb/J transgenic donor mice (Jackson Laboratory, Bar Habor, ME). BM cells were harvested aseptically by flushing the tibias and femurs of adult animals and subjected to erythrocytes lysis. After BM reconstitution (4-6 weeks post-irradiation) B16F10 cells were subcutaneously implanted into the flanks of the mice. Two or 28 days later animals were sacrificed and lungs were isolated and lung histology was performed. All procedures involving mice were approved by the local institutional Animal Care Committee (Regierungspräsidium Düsseldorf Az84-02.04.2012.A137; 84-02.04.2012.A034). The Mmp2 inhibitor ARP100 (sc203522, CAS 704888-90-4) was from Santa Cruz (Santa Cruz, CA).

Stock solutions of ARP100 were prepared by dissolving 5mg ARP100 in 200µl sterile DMSO. The stock solution was further diluted with sterile PBS for *in vivo* application. Intraperitoneal injections of ARP100 were given twice weekly at a final concentration of 15µg/g bodyweight (e.g. 15µl ARP100 stock solution + 85µl PBS per injection per mouse with a bodyweight of 25 g).

Isolation and purification of aortic MSCs and bone marrow MSCs

Vascular wall resident MSC were isolated from aortas of C57BL/6-Tg(CAG-EGFP)1Osb/J mice (Jackson Laboratory, Bar Habor, ME) as previously described (40). In brief, tissue pieces were mechanically minced and dissociated for 15 minutes at 37°C in OptiMEM I medium containing 0.2% type 2-collagenase (CLS2, 43J14367B, ≥125 units per mg dry weight; Worthington, Lakewood, WA). Cells were washed twice in PBS/ 5% FCS. Pure MSCs were generated using a Sca-1 antibody (130-092-529) and MACS technology (Miltenyi Biotec, Bergisch Gladbach, Germany) according to the manufacturer's instructions. Primary MSCs were cultivated on plastic plates in DMEM/20% FCS. Medium was removed 24 hours after initial plating and non-adherent cells were washed away. Primary cultures were clonally expanded under limiting dilution conditions. BM cells were harvested and cultured using complete DMEM/ 20% FCS as previously described (40).

Vascular leakage

Twenty-one days after irradiation vascular leakage was determined by Evans blue dye (EBD, E2129, Sigma-Aldrich, St. Louis, MO) or Alexa555-labelled BSA (A34786, Life Technologies, Carlsbad, CA) extravasation from the blood stream into the lung interstitium. Therefore 100µg EBD or 50µg Alexa555-BSA/ 100µl PBS were intravenously injected into the tail vein. Two to four hours after injection animals received a deep anesthesia and were sacrificed by transcardial perfusion with PBS to remove the blood from the vascular system. Lungs were isolated and subjected for protein isolation and EBD extraction. Lung pieces were weighted and EBD exuded in the lung interstitium was extracted by incubating the tissue in 200µl formamide for 24 h at 65 °C, and dye concentrations were measured by absorption at 620

nm and related to the weight of lung tissue (µg of EBD per mg wet weight of the lung). Alexa555-BSA concentrations were determined by measuring fluorescence at 555 nm.

.

Western blot

Whole cell lysates were generated by scraping cells into ice-cold RIPA-P buffer (150 mmol/L NaCl, 1% NP40, 0.5% sodium-desoxycholate, 0.1% sodium-dodecylsulfate, 50 mmol/L Tris/HCL pH8, 10 mmol/L sodium fluoride (NaF), 1 mmol/L sodium orthovandanate (Na_3VO_4) supplemented with complete Protease-Inhibitor-Cocktail (04693159001, Hoffmann-La Roche, Basel, Switzerland) and performing 2–3 freeze-thaw cycles. Protein samples (50–100 µg total protein) were subjected to SDS-PAGE electrophoresis and Western blots were done as previously described using indicated antibodies (39). Mmp2 (H76, sc10736), p21 (F8, sc271610) and VE-Cad (C19, sc6458) antibodies were from Santa Cruz (Santa Cruz, CA), pTyr (P-Tyr-100, 9411S) antibody was from New England Biolabs (Ipswich, MA).

Real-time RT-PCR

RNA was isolated using RNeasy Mini Kit (74106, Qiagen, Hilden, Germany) according to the manufacturer's instruction and as previously described (38,39). Expression levels were normalized to the reference gene (beta actin; set as 1) and are shown as relative quantification. Specific primers were synthesized based on available sequences for each listened gene. Primer design was done with the program Primer 3 (http://frodo.wi.mit.edu/cgi-bin/primer3/primer3_www.cgi). Cross-reaction of primers with the genes was excluded by comparison of the sequence of interest with a database (Blast 2.2, U.S. National Centre for Biotechnology Information, Bethesda, MD) and all primers used in our study were intron-spanning. PCR products are 200-300 bp in size. Quantitative Real-Time RT-PCR was carried out using the specific oligonucleotide primers (Mmp2fw- gctccaccacatacaactttga, Mmp2bw-tcgggacagaatccatacttct, Mmp14fw-gcatccatcaatactgcctac, Mmp14bw-tagtacttattgccccggaaga, Timp2fw-agaagaagagcctgaaccacag, Timp2bw-ggtcctcgatgtcaagaaactc, Ccl2fw-gggcctgctgttcacagt, Ccl2bw- cctactcattgggatcatcttgct,

Plaufw- aaatggtgactcttaccgagga, Plaubw-taagagagcagtcatgcaccat) as previously described (38,39).

Immunohistochemistry and electron microscopy

Paraffin-embedded tissue sections were hydrated using a descending alcohol series, incubated for 10–20 min in target retrieval solution (DAKO, Glostrup, Denmark) and incubated with blocking solution (2% FCS/PBS). After permeabilisation, sections were incubated over night at 4°C with primary antibodies [Mmp2 (H76, sc10736), Plau/uPA (uPa; H-140, sc14019) both from Santa Cruz (Santa Cruz, CA) and Ccl2 (AA102-130, ABIN1108186) from antibodies-online (Atlanta, GA)]. Antigen was detected with an alkaline phosphatase-conjugated secondary antibody (1/250) and ALP staining (DAKO, Glostrup, Denmark). Nuclei were counterstained using hematoxylin. For fluorescence analysis [VE-Cad (C19, sc6458 from Santa Cruz, Santa Cruz, CA), CD31 (DIA-310; Dianova, Hamburg, Germany)] the antigens were detected with anti-rat-Alexa488 and anti-mouse-Alexa555-conjugated secondary antibodies (1/500) as previously described (41). Hoechst 33342 (H1399, Life Technologies, Carlsbad, CA) was used for staining of nuclei. Electron microscopy was done as previously described (41).

Senescence-associated beta-galactosidase (SA-βgal) activity

Senescence-associated beta-galactosidase (SA-betagal) activity was detected as previously described using frozen sections of lung tissue at pH 6.0 (19). In brief, for the X-gal (5-bromo-4-chloro-3-indolyl-β-D-galactopyranoside, B4252 Sigma-Aldrich, St. Louis, MO) staining procedure all working solutions were freshly prepared. Slides were fixed in 4% PFA for 30 min at 4°C, rinsed with wash buffer for 4 × 5 min and developed by incubation of slides with X-gal staining solution (containing 0.1% X-gal, 5 mM potassium ferrocyanide, 5 mM potassium ferricyanide, 150 mM Sodium chloride, and 2 mM magnesium chloride in 40 mM citric acid/sodium phosphate solution, pH 6.0) for more than 12 h in 37°C incubator. The staining container was impermeable to normal light. After overnight staining, slides were

washed with PBS 3 × 5 min. All chemicals were from Sigma-Aldrich (St. Louis, MO) if not otherwise indicated.

Lung histopathology

For lung histology mice were narcotized using isoflurane (2-chloro-2-(difluoromethoxy)-1,1,1-trifluoro-ethane) and killed by transcardial perfusion with PBS. Whole lungs were taken out and lung tissue was fixed in 4% formalin and subsequently embedded in paraffin. Three to four 5-µm paraffin longitudinal cross-sections were taken per mouse lung at the midpoint through the lung block depth. Sections were stained with hematoxylin and eosin for histological evaluation. Samples were then analyzed microscopically with a 20× objective. Metastatic lesions/foci were quantified by counting numbers of nodules in at least 3 whole cross-sections per lung and averages for individual animals were calculated. Depicted data represent the mean values of all mice per group (mean of single average number for each mouse/ mouse number) as indicated.

Phenotyping of lung leukocytes by flow cytometry

Crude cell extracts of freshly isolated lungs were generated and FACS analysis was performed as previously described (69). Lung cell suspensions were stained with anti-mouse CD45 (30-F11; Cat. 103126) for determination of leukocytes in the lung tissue. Lung cells were further fluorochrome-labeled with anti-mouse Ly6C (HK1.4; Cat. 128006), CD11b (M1/70; Cat. 101228), and CD11c (N418; Cat. 117309). All antibodies used in this study were obtained from BioLegend (San Diego, CA), respectively. Flow cytometric measurements were performed on a BD LSRII flow cytometer using FACS DIVA software. Analysis of data sets was done using BD CellQuest Pro software (all from BD Bioscience, Franklin Lakes, NJ).

Statistical Analysis

If not otherwise indicated, data were obtained from 3 independent experiments with at least 3 mice each. Mean values were calculated and used for analysis of standard error (SEM) as

indicated by error bars. Statistical significance was evaluated by 1-way or 2-way ANOVA followed by Bonferroni's multiple comparison post-test. Statistical significance was set at the level of $P \leq 0.05$. Data analysis was performed with Prism 5.0 software (GraphPad, La Jolla, CA).

Acknowledgements

We thank L. Lüdemann and M. Groneberg for support with the irradiation of mice, Mohamed Benchellal, Inge Spratte and Eva Gau for their excellent technical assistance. The work was supported by grants of the DFG (GRK1739/1; JE275/1) the BMBF (ZISS 02NUK024-D), and the UK Essen/IFORES (D/107-81040). Contributions: D.K., A.S., R.I. and F.W. and K.U. performed experiments, H.J. performed electron microscopy, D.K. supervised and analysed results and made the figures; K.U. and M.S. provided materials; D.K. and V.J. designed research and wrote the paper. All authors read and approved the manuscript.

Author Disclosure Statement

The authors state that there are no personal or institutional conflicts of interest.

List of Abbreviations

ALP	alkaline phasphatase
Ao	aorta
BM	bone marrow
Ccl2	chemokine (C-C motif) ligand 2
DMEM	Dulbecco's Modified Eagle's Medium
DMSO	Dimethylsulfoxide
EBD	Evans blue dye
EC	endothelial cell
EGFP	enhanced green fluorescent protein
FCS	fetal calf serum
GM-CSF	Granulocyte-macrophage colony-stimulating factor
Gy	Gray
IR	ionizing radiation
IHC	immunohistochemistry
MLEC	mouse lung endothelial cells
Mmp2	matrix metalloproteinase 2
Mmp14	matrix metalloproteinase 14
MSC	multipotent stem cell
MSC	mesenchymal stem cell
PBS	phosphate buffered saline
Plau/uPA	urokinase-type plasminogen activator
RT	radiotherapy
SASP	senescence-associated secretory phenotype
SD	standard deviation
SEM	standard errorof the mean
Timp2	tissue inhibitor of metalloproteinases 2
TS/A	metastasizing cell line from a BALB/c spontaneous mammary adenocarcinoma

VE-Cad vascular endothelial cadherin

WTI Whole thorax irradiation

References

1. Ahn GO, Tseng D, Liao CH, Dorie MJ, Czechowicz A, Brown JM. Inhibition of Mac-1 (CD11b/CD18) enhances tumor response to radiation by reducing myeloid cell recruitment. *Proc Natl Acad Sci U S A* 107: 8363-8, 2010.
2. Angelini PD, Zacarias Fluck MF, Pedersen K, Parra-Palau JL, Guiu M, Bernado Morales C, Vicario R, Luque-Garcia A, Navalpotro NP, Giralt J, Canals F, Gomis RR, Tabernero J, Baselga J, Villanueva J, Arribas J. Constitutive HER2 signaling promotes breast cancer metastasis through cellular senescence. *Cancer Res* 73: 450-8, 2013.
3. Balermpas P, Michel Y, Wagenblast J, Seitz O, Weiss C, Rodel F, Rodel C, Fokas E. Tumour-infiltrating lymphocytes predict response to definitive chemoradiotherapy in head and neck cancer. *Br J Cancer* 110: 501-9, 2014.
4. Bang OY, Lee JS, Lee PH, Lee G. Autologous mesenchymal stem cell transplantation in stroke patients. *Ann Neurol* 57: 874-82, 2005.
5. Barcellos-Hoff MH, Park C, Wright EG. Radiation and the microenvironment - tumorigenesis and therapy. *Nat Rev Cancer* 5: 867-75, 2005.
6. Benderitter M, Caviggioli F, Chapel A, Coppes RP, Guha C, Klinger M, Malard O, Stewart F, Tamarat R, Luijk PV, Limoli CL. Stem cell therapies for the treatment of radiation-induced normal tissue side effects. *Antioxid Redox Signal* 21: 338-55, 2014.
7. Bernier J, Hall EJ, Giaccia A. Radiation oncology: a century of achievements. *Nat Rev Cancer* 4: 737-47, 2004.
8. Campisi J, d'Adda di Fagagna F. Cellular senescence: when bad things happen to good cells. *Nat Rev Mol Cell Biol* 8: 729-40, 2007.
9. Cappuccini F, Eldh T, Bruder D, Gereke M, Jastrow H, Schulze-Osthoff K, Fischer U, Kohler D, Stuschke M, Jendrossek V. New insights into the molecular pathology of radiation-induced pneumopathy. *Radiother Oncol* 101: 86-92, 2011.
10. Chin SP, Poey AC, Wong CY, Chang SK, Teh W, Mohr TJ, Cheong SK. Cryopreserved mesenchymal stromal cell treatment is safe and feasible for severe dilated ischemic cardiomyopathy. *Cytotherapy* 12: 31-7, 2010.
11. Chung YL, Jian JJ, Cheng SH, Tsai SY, Chuang VP, Soong T, Lin YM, Horng CF. Sublethal irradiation induces vascular endothelial growth factor and promotes growth of hepatoma cells: implications for radiotherapy of hepatocellular carcinoma. *Clin Cancer Res* 12: 2706-15, 2006.
12. Conese M, Carbone A, Castellani S, Di Gioia S. Paracrine effects and heterogeneity of marrow-derived stem/progenitor cells: relevance for the treatment of respiratory diseases. *Cells Tissues Organs* 197: 445-73, 2013.
13. Copland IB. Mesenchymal stromal cells for cardiovascular disease. *J Cardiovasc Dis Res* 2: 3-13, 2011.
14. Coppe JP, Desprez PY, Krtolica A, Campisi J. The senescence-associated secretory phenotype: the dark side of tumor suppression. *Annu Rev Pathol* 5: 99-118, 2010.
15. Coppe JP, Patil CK, Rodier F, Sun Y, Munoz DP, Goldstein J, Nelson PS, Desprez PY, Campisi J. Senescence-associated secretory phenotypes reveal cell-nonautonomous functions of oncogenic RAS and the p53 tumor suppressor. *PLoS Biol* 6: 2853-68, 2008.
16. Coppes RP, van der Goot A, Lombaert IM. Stem cell therapy to reduce radiation-induced normal tissue damage. *Semin Radiat Oncol* 19: 112-21, 2009.
17. Craig MJ, Loberg RD. CCL2 (Monocyte Chemoattractant Protein-1) in cancer bone metastases. *Cancer Metastasis Rev* 25: 611-9, 2006.
18. Cummings B, Keane T, Pintilie M, Warde P, Waldron J, Payne D, Liu FF, Bissett R, McLean M, Gullane P, O'Sullivan B. Five year results of a randomized trial comparing hyperfractionated to conventional radiotherapy over four weeks in locally advanced head and neck cancer. *Radiother Oncol* 85: 7-16, 2007.
19. Debacq-Chainiaux F, Erusalimsky JD, Campisi J, Toussaint O. Protocols to detect senescence-associated beta-galactosidase (SA-betagal) activity, a biomarker of senescent cells in culture and in vivo. *Nat Protoc* 4: 1798-806, 2009.
20. Eldh T, Heinzelmann F, Velalakan A, Budach W, Belka C, Jendrossek V. Radiation-induced changes in breathing frequency and lung histology of C57BL/6J mice are time- and dose-dependent. *Strahlenther Onkol* 188: 274-81, 2012.

21. Ergun S, Tilki D, Klein D. Vascular wall as a reservoir for different types of stem and progenitor cells. *Antioxid Redox Signal* 15: 981-95, 2011.
22. Garcia-Barros M, Paris F, Cordon-Cardo C, Lyden D, Rafii S, Haimovitz-Friedman A, Fuks Z, Kolesnick R. Tumor response to radiotherapy regulated by endothelial cell apoptosis. *Science* 300: 1155-9, 2003.
23. Ghafoori P, Marks LB, Vujaskovic Z, Kelsey CR. Radiation-induced lung injury. Assessment, management, and prevention. *Oncology (Williston Park)* 22: 37-47; discussion 52-3, 2008.
24. Ghobadi G, Bartelds B, van der Veen SJ, Dickinson MG, Brandenburg S, Berger RM, Langendijk JA, Coppes RP, van Luijk P. Lung irradiation induces pulmonary vascular remodelling resembling pulmonary arterial hypertension. *Thorax* 67: 334-41, 2012.
25. Gil-Bernabe AM, Ferjancic S, Tlalka M, Zhao L, Allen PD, Im JH, Watson K, Hill SA, Amirkhosravi A, Francis JL, Pollard JW, Ruf W, Muschel RJ. Recruitment of monocytes/macrophages by tissue factor-mediated coagulation is essential for metastatic cell survival and premetastatic niche establishment in mice. *Blood* 119: 3164-75, 2012.
26. Gotherstrom C, West A, Liden J, Uzunel M, Lahesmaa R, Le Blanc K. Difference in gene expression between human fetal liver and adult bone marrow mesenchymal stem cells. *Haematologica* 90: 1017-26, 2005.
27. Graves PR, Siddiqui F, Anscher MS, Movsas B. Radiation pulmonary toxicity: from mechanisms to management. *Semin Radiat Oncol* 20: 201-7, 2010.
28. Grizzle WE, Mountz JD, Yang PA, Xu X, Sun S, Van Zant GE, Williams RW, Hsu HC, Zhang HG. BXD recombinant inbred mice represent a novel T cell-mediated immune response tumor model. *Int J Cancer* 101: 270-9, 2002.
29. Hamalukic M, Huelsenbeck J, Schad A, Wirtz S, Kaina B, Fritz G. Rac1-regulated endothelial radiation response stimulates extravasation and metastasis that can be blocked by HMG-CoA reductase inhibitors. *PLoS One* 6: e26413, 2011.
30. Hass R, Kasper C, Bohm S, Jacobs R. Different populations and sources of human mesenchymal stem cells (MSC): A comparison of adult and neonatal tissue-derived MSC. *Cell Commun Signal* 9: 12, 2011.
31. He Q, Wan C, Li G. Concise review: multipotent mesenchymal stromal cells in blood. *Stem Cells* 25: 69-77, 2007.
32. Hoang T, Huang S, Armstrong E, Eickhoff JC, Harari PM. Enhancement of radiation response with bevacizumab. *J Exp Clin Cancer Res* 31: 37, 2012.
33. Hoffman AM, Paxson JA, Mazan MR, Davis AM, Tyagi S, Murthy S, Ingenito EP. Lung-derived mesenchymal stromal cell post-transplantation survival, persistence, paracrine expression, and repair of elastase-injured lung. *Stem Cells Dev* 20: 1779-92, 2011.
34. Jin HJ, Bae YK, Kim M, Kwon SJ, Jeon HB, Choi SJ, Kim SW, Yang YS, Oh W, Chang JW. Comparative analysis of human mesenchymal stem cells from bone marrow, adipose tissue, and umbilical cord blood as sources of cell therapy. *Int J Mol Sci* 14: 17986-8001, 2013.
35. Kaplan RN, Rafii S, Lyden D. Preparing the "soil": the premetastatic niche. *Cancer Res* 66: 11089-93, 2006.
36. Kargozaran H, Yuan SY, Breslin JW, Watson KD, Gaudreault N, Breen A, Wu MH. A role for endothelial-derived matrix metalloproteinase-2 in breast cancer cell transmigration across the endothelial-basement membrane barrier. *Clin Exp Metastasis* 24: 495-502, 2007.
37. Kern S, Eichler H, Stoeve J, Kluter H, Bieback K. Comparative analysis of mesenchymal stem cells from bone marrow, umbilical cord blood, or adipose tissue. *Stem Cells* 24: 1294-301, 2006.
38. Klein D, Benchellal M, Kleff V, Jakob HG, Ergun S. Hox genes are involved in vascular wall-resident multipotent stem cell differentiation into smooth muscle cells. *Sci Rep* 3: 2178, 2013.
39. Klein D, Demory A, Peyre F, Kroll J, Augustin HG, Helfrich W, Kzhyshkowska J, Schledzewski K, Arnold B, Goerdt S. Wnt2 acts as a cell type-specific, autocrine growth factor in rat hepatic sinusoidal endothelial cells cross-stimulating the VEGF pathway. *Hepatology* 47: 1018-31, 2008.
40. Klein D, Meissner N, Kleff V, Jastrow H, Yamaguchi M, Ergun S, Jendrossek V. Nestin(+) tissue-resident multipotent stem cells contribute to tumor progression by differentiating into pericytes and smooth muscle cells resulting in blood vessel remodeling. *Front Oncol* 4: 169, 2014.
41. Klein D, Weisshardt P, Kleff V, Jastrow H, Jakob HG, Ergun S. Vascular wall-resident CD44+ multipotent stem cells give rise to pericytes and smooth muscle cells and contribute to new vessel maturation. *PLoS One* 6: e20540, 2011.
42. Krtolica A, Parrinello S, Lockett S, Desprez PY, Campisi J. Senescent fibroblasts promote epithelial cell growth and tumorigenesis: a link between cancer and aging. *Proc Natl Acad Sci U S A* 98: 12072-7, 2001.

43. Le ON, Rodier F, Fontaine F, Coppe JP, Campisi J, DeGregori J, Laverdiere C, Kokta V, Haddad E, Beausejour CM. Ionizing radiation-induced long-term expression of senescence markers in mice is independent of p53 and immune status. *Aging Cell* 9: 398-409, 2010.
44. Liang H, Deng L, Chmura S, Burnette B, Liadis N, Darga T, Beckett MA, Lingen MW, Witt M, Weichselbaum RR, Fu YX. Radiation-induced equilibrium is a balance between tumor cell proliferation and T cell-mediated killing. *J Immunol* 190: 5874-81, 2013.
45. Luan Y, Zhang ZH, Wei DE, Zhao JJ, Kong F, Cheng GH, Wang YB. Implantation of mesenchymal stem cells improves right ventricular impairments caused by experimental pulmonary hypertension. *Am J Med Sci* 343: 402-6, 2012.
46. McNulty K, Janes SM. Stem cells and pulmonary fibrosis: cause or cure? *Proc Am Thorac Soc* 9: 164-71, 2012.
47. Min HJ, Lee Y, Zhao XF, Park YK, Lee MK, Lee JW, Kim S. TMPRSS4 upregulates uPA gene expression through JNK signaling activation to induce cancer cell invasion. *Cell Signal* 26: 398-408, 2014.
48. Muller M. Cellular senescence: molecular mechanisms, in vivo significance, and redox considerations. *Antioxid Redox Signal* 11: 59-98, 2009.
49. Munshi HG, Stack MS. Reciprocal interactions between adhesion receptor signaling and MMP regulation. *Cancer Metastasis Rev* 25: 45-56, 2006.
50. Mureli S, Gans CP, Bare DJ, Geenen DL, Kumar NM, Banach K. Mesenchymal stem cells improve cardiac conduction by upregulation of connexin 43 through paracrine signaling. *Am J Physiol Heart Circ Physiol* 304: H600-9, 2013.
51. Pittenger MF, Mackay AM, Beck SC, Jaiswal RK, Douglas R, Mosca JD, Moorman MA, Simonetti DW, Craig S, Marshak DR. Multilineage potential of adult human mesenchymal stem cells. *Science* 284: 143-7, 1999.
52. Ruegg C, Monnier Y, Kuonen F, Imaizumi N. Radiation-induced modifications of the tumor microenvironment promote metastasis. *Bull Cancer* 98: 47-57, 2011.
53. Sarvaiya PJ, Guo D, Ulasov I, Gabikian P, Lesniak MS. Chemokines in tumor progression and metastasis. *Oncotarget* 4: 2171-85, 2013.
54. Shen Q, Lee ES, Pitts RL, Wu MH, Yuan SY. Tissue inhibitor of metalloproteinase-2 regulates matrix metalloproteinase-2-mediated endothelial barrier dysfunction and breast cancer cell transmigration through lung microvascular endothelial cells. *Mol Cancer Res* 8: 939-51, 2010.
55. Shimizu K, Kinouchi Shimizu N, Asai T, Tsukada H, Oku N. Enhanced experimental tumor metastasis with age in senescence-accelerated mouse. *Biol Pharm Bull* 31: 847-51, 2008.
56. Shin JW, Son JY, Raghavendran HR, Chung WK, Kim HG, Park HJ, Jang SS, Son CG. High-dose ionizing radiation-induced hematotoxicity and metastasis in mice model. *Clin Exp Metastasis* 28: 803-10, 2011.
57. Slavin S, Kurkalli BG, Karussis D. The potential use of adult stem cells for the treatment of multiple sclerosis and other neurodegenerative disorders. *Clin Neurol Neurosurg* 110: 943-6, 2008.
58. Stewart DJ, Mei SH. Cell-based therapies for lung vascular diseases: lessons for the future. *Proc Am Thorac Soc* 8: 535-40, 2011.
59. Tchkonia T, Zhu Y, van Deursen J, Campisi J, Kirkland JL. Cellular senescence and the senescent secretory phenotype: therapeutic opportunities. *J Clin Invest* 123: 966-72, 2013.
60. Tsoutsou PG, Koukourakis MI. Radiation pneumonitis and fibrosis: mechanisms underlying its pathogenesis and implications for future research. *Int J Radiat Oncol Biol Phys* 66: 1281-93, 2006.
61. Tzouvelekis A, Antoniadis A, Bouros D. Stem cell therapy in pulmonary fibrosis. *Curr Opin Pulm Med* 17: 368-73, 2011.
62. Tzouvelekis A, Koliakos G, Ntolios P, Baira I, Bouros E, Oikonomou A, Zissimopoulos A, Kolios G, Kakagia D, Paspaliaris V, Kotsianidis I, Froudarakis M, Bouros D. Stem cell therapy for idiopathic pulmonary fibrosis: a protocol proposal. *J Transl Med* 9: 182, 2011.
63. Tzouvelekis A, Ntolios P, Bouros D. Stem cell treatment for chronic lung diseases. *Respiration* 85: 179-92, 2013.
64. van Deventer HW, Palmieri DA, Wu QP, McCook EC, Serody JS. Circulating fibrocytes prepare the lung for cancer metastasis by recruiting Ly-6C+ monocytes via CCL2. *J Immunol* 190: 4861-7, 2013.
65. Wan L, Pantel K, Kang Y. Tumor metastasis: moving new biological insights into the clinic. *Nat Med* 19: 1450-64, 2013.
66. Wang L, Fan J, Thompson LF, Zhang Y, Shin T, Curiel TJ, Zhang B. CD73 has distinct roles in nonhematopoietic and hematopoietic cells to promote tumor growth in mice. *J Clin Invest* 121: 2371-82, 2011.
67. Wels J, Kaplan RN, Rafii S, Lyden D. Migratory neighbors and distant invaders: tumor-associated niche cells. *Genes Dev* 22: 559-74, 2008.

68. Wen Z, Zheng S, Zhou C, Wang J, Wang T. Repair mechanisms of bone marrow mesenchymal stem cells in myocardial infarction. *J Cell Mol Med* 15: 1032-43, 2011.
69. Wirsdorfer F, Cappuccini F, Niazman M, de Leve S, Westendorf AM, Ludemann L, Stuschke M, Jendrossek V. Thorax irradiation triggers a local and systemic accumulation of immunosuppressive CD4+ FoxP3+ regulatory T cells. *Radiat Oncol* 9: 98, 2014.
70. Zaleska K, Bruechner K, Baumann M, Zips D, Yaromina A. Tumour-infiltrating CD11b+ myelomonocytes and response to fractionated irradiation of human squamous cell carcinoma (hSCC) xenografts. *Radiother Oncol* 101: 80-5, 2011.
71. Zeng L, Ou G, Itasaka S, Harada H, Xie X, Shibuya K, Kizaka-Kondoh S, Morinibu A, Shinomiya K, Hiraoka M. TS-1 enhances the effect of radiotherapy by suppressing radiation-induced hypoxia-inducible factor-1 activation and inducing endothelial cell apoptosis. *Cancer Sci* 99: 2327-35, 2008.
72. Zhang H, Fang J, Wu Y, Mai Y, Lai W, Su H. Mesenchymal stem cells protect against neonatal rat hyperoxic lung injury. *Expert Opin Biol Ther* 13: 817-29, 2013.
73. Zhang Y, Liao S, Yang M, Liang X, Poon MW, Wong CY, Wang J, Zhou Z, Cheong SK, Lee CN, Tse HF, Lian Q. Improved cell survival and paracrine capacity of human embryonic stem cell-derived mesenchymal stem cells promote therapeutic potential for pulmonary arterial hypertension. *Cell Transplant* 21: 2225-39, 2012.
74. Zhao S, Wehner R, Bornhauser M, Wassmuth R, Bachmann M, Schmitz M. Immunomodulatory properties of mesenchymal stromal cells and their therapeutic consequences for immune-mediated disorders. *Stem Cells Dev* 19: 607-14, 2010.
75. Zhu Y, Yang Y, Zhang Y, Hao G, Liu T, Wang L, Yang T, Wang Q, Zhang G, Wei J, Li Y. Placental mesenchymal stem cells of fetal and maternal origins demonstrate different therapeutic potentials. *Stem Cell Res Ther* 5: 48, 2014.

Figure Legends

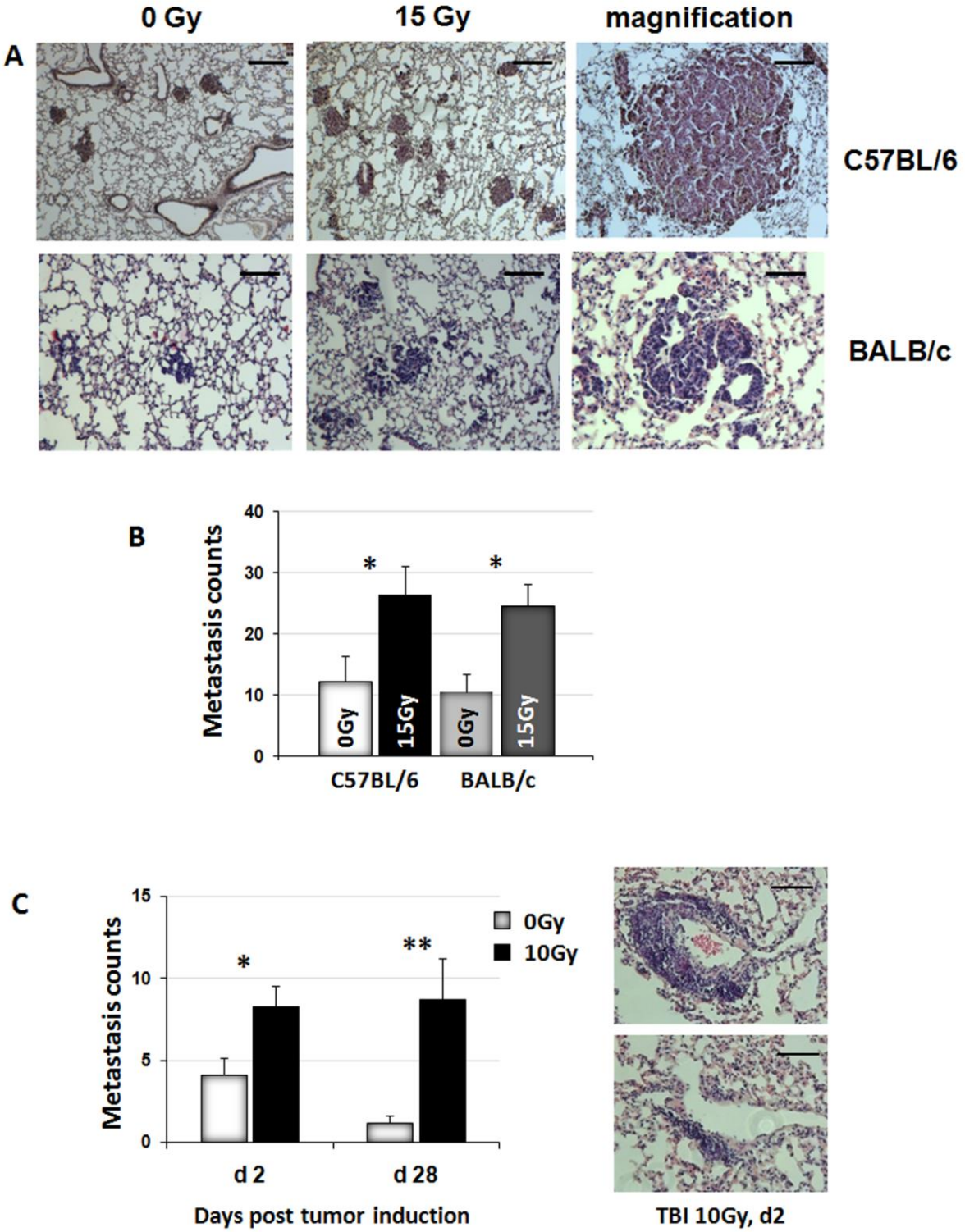

Figure 1

Ionizing irradiation increases metastasis formation in previously irradiated lung tissue

(A) Wild type C57BL/6 and BALB/c mice received 15 Gray of whole thorax irradiation (WTI). Seeding of circulating tumor cells into the lungs was initiated 21 days after irradiation. Therefore, 1*10(6) B16F10 cells were intravenously transplanted via the tail vein of C57BL/6

mice and 1*10(6) TS/A cells into BALB/c mice. Fourteen days after tumor cell injection animals were sacrificed, lungs were isolated and subjected for lung histopathology. Photographs show an increased formation of metastasis in irradiated lungs 14 days after tumor cell injection in both mouse strains. Scalebar = 100 µm, magnification scale bar = 25µm. (**B**) Lung metastasis formation was assessed and counted in whole lung sections after hematoxylin staining. Data are presented as mean ± SEM from three independent experiments (C57BL6/15Gy: n= 10; 0Gy: n= 13; BALB/c 15Gy: n= 11; 0Gy: n= 9). P-values were indicated: *$P \leq 0.05$ by two-way ANOVA followed by post-hoc Bonferroni test. (**C**) B16F10 tumor cells were subcutaneously transplanted into the flank of bone marrow reconstituted C57BL/6 mice after a lethal total body irradiation (TBI; splitting dose 7 + 3 Gy). After a survival time of 2 or 28 days animals were sacrificed, tissues were isolated and subjected to histopathological analysis. Photomicrographs visualize the increased metastatic spread to previously irradiated lungs in mice bearing subcutaneously growing tumors. Scalebar = 20 µm. Quantification of tumor cell extravasation (here designated as micrometastasis) and subsequently formed macrometastasis was performed in hematoxylin stained whole lung sections (left panel); data are presented as mean ± SEM from four independent experiments (28d/ 10Gy: n = 22; 0Gy: n = 11; 2d/ 15Gy: n = 18; 0Gy: n = 11). P-values were indicated: *$P \leq 0.05$, **$P \leq 0.01$ by two-way ANOVA followed by post-hoc Bonferroni test. “(To see this illustration in color the reader is referred to the web version of this article at www.liebertonline.com/ars)”

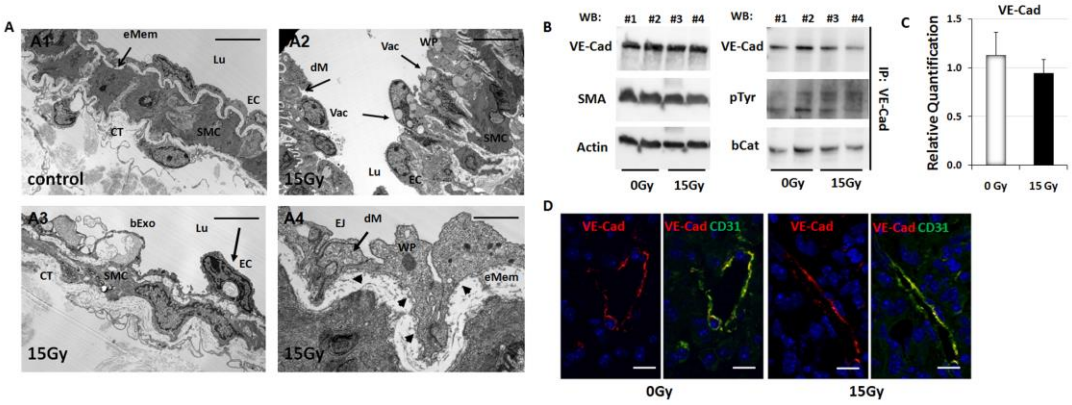

Figure 2

Thorax-irradiation induces vascular endothelial cell damage

(**A**) Mice were irradiated over the whole thorax (single fraction 15Gy WTI), sacrificed 21 days after radiation and lungs were subjected to electron microscopic analysis (n = 3 per group). Sham control animals underwent the same procedure without irradiation. A defective and irregular basement membrane lining arterial endothelial cells (EC) is emphasized by arrow heads. Partially degraded mitochondria (dM) and numerous vacuoles (Vac) present in EC are indicated by arrows. SMC smooth muscle cell, eMem elastic membrane, WP Weibel Palade bodies, bExo Basolateral exocytosis, CT connective tissue, Lu lumen, EJ endothelial cell junctions. Scale bar: A1-A3 = 10 µm, A4 = 2µm) (**B**) To confirm the regular arrangement of endothelial cell junctions (EJ in panel A4) the total amount of VE-cadherin (VE-Cad; left panel) as well as its low phosphorylation status and the proper association with beta-catenin was demonstrated by co-immunoprecipitation of VE-Cad (IP: VE-Cad; right panel) and Western blot analysis of protein cell lysates obtained from whole mouse lungs. Beta-actin was included as a loading control. The different IP-samples were divided into two and loaded on two different gels (with equal protein amounts used. One membrane was used for incubation with the first antibody (anti pTyr) and afterwards reprobed with anti VE-Cad. The second gel was incubated with anti beta-catenin antibody (#, different animals, SMA smooth muscle actin, pTyr phosphotyrosine). (**C**) Real-Time RT-PCR quantification of *VE-Cad* mRNA expression in total lung RNA isolates derived 21 days after irradiation from control as well as WTI animals was performed. Expression levels were normalized to the reference gene (beta Actin) and are shown as relative quantification. (**D**) Cell surface localization of

VE-Cad in lung endothelial cells was further confirmed by immunocolocalization of VE-Cad (red) and CD31 (green) expressions. Representative images of three independent experiments are shown. Scale bar = 10 μm. “(To see this illustration in color the reader is referred to the web version of this article at www.liebertonline.com/ars)”

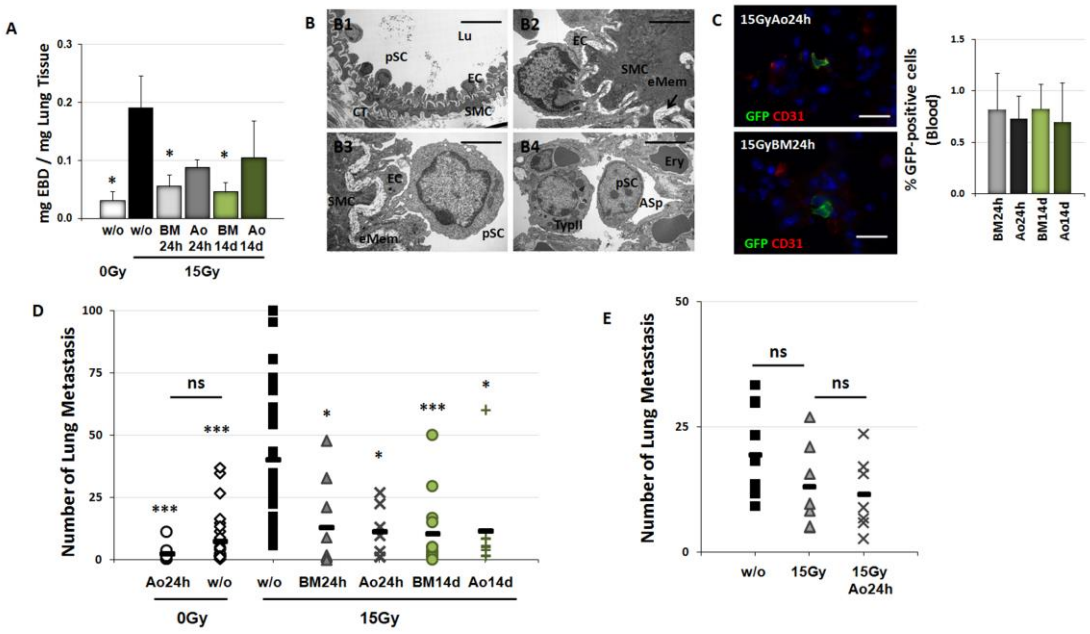

Figure 3

MSC-therapy normalizes endothelial cell morphology and vascular function and limits lung metastasis after thorax irradiation

C57BL/6 mice were left untreated or received a 15Gy WTI. Single cell suspensions of cultured MSCs (0.5*10(6) cells) derived from the aorta (Ao) or from the bone marrow (BM) were intravenously transplanted into the tail vain of control or WTI mice 24 hours or 14 days after irradiation as indicated (five mice per group). (**A**) After 21 days vascular leakage was determined by Evans blue dye extravasation (EBD) from the blood stream to the lung interstitium. Dye concentrations in the isolated lungs were quantified by absorption measurements and related to the weight of lung tissue. P-values indicate: *$P \leq 0.05$ (n = 5) by one-way ANOVA followed by post-hoc Bonferroni test. (**B**) Morphological analysis of lung blood vessels was done using electron microscopy. Scale bar B1 = 20 µm, B2-B4 = 5 µm. A regular vessel structure as well as endothelial cell (EC) morphology was present in the lungs of MSC-treated animals (B1-4). Ultrastructural analysis further demonstrated a normalized presence of undifferentiated cells (putative stem cells, pSC) in the blood stream as well as in the alveolar space. SMC smooth muscle cell, eMem elastic membrane, WP Weibel Palade bodies, Ery erythrocytes, ASp alveolar space, Lu lumen, TypII alveolar epithelial cell type II, CT connective tissue. (**C**) 21 days after irradiation immunofluorescence staining for GFP

(green) and CD31 (red) on lung sections was performed (left panel). Scale bar = 20 µm. Peripheral blood samples were obtained 25 weeks after irradiation and circulating GFP+ MSCs were quantified via flow cytometry. No GFP expression was detected in the control (0Gy) and WTI-irradiated animals (15Gy). Data are presented as mean ± SEM (5-7 animals per group; right panel). Data is not significant as analyzed by two-way ANOVA followed by post-hoc Bonferroni test. (**D**) Seeding of circulating tumor cells into the lungs was analyzed 21 days after irradiation and MSC application (BM/Ao24h, BM/Ao14d) by intravenously injection of 1*10(6) B16F10 cells into the tail vein. Sham-irradiated and AoMSC-treated animals served as controls (0GyAo24h). After 14 days of tumor cell injection animals were sacrificed, lungs were isolated and subjected for lung histology. Lung metastasis formation was quantified in whole lung sections. Shown are mean values of three different experiments with a minimum of 8 animals per group (90 mice in total). Symbols depict single mice. P-values were indicated: $*P \leq 0.05$, $**P \leq 0.01$, $***P \leq 0.001$ by two-way ANOVA followed by post-hoc Bonferroni test (comparison to 15Gy). (**E**) To further rule out that MSC-therapy had no metastasis promoting affects on previously grown tumors, untreated C57BL/6 mice were intravenously injected with 2*10(6) B16F10 cells into the tail vein and metastasis formation and growth was allowed for 14 days (animal group w/o). Two sets of animals received subsequently a 15Gy-WTI and one set in addition a single cell suspension of cultured MSCs (0.5*10(6) cells) derived from the aorta (15GyAo24h). After another 21 days animals were sacrificed and lungs metastasis formation was quantified in whole lung sections (w/o: n = 10; 15Gy: n = 7; 15GyAo24h: n = 7). “(To see this illustration in color the reader is referred to the web version of this article at www.liebertonline.com/ars)”

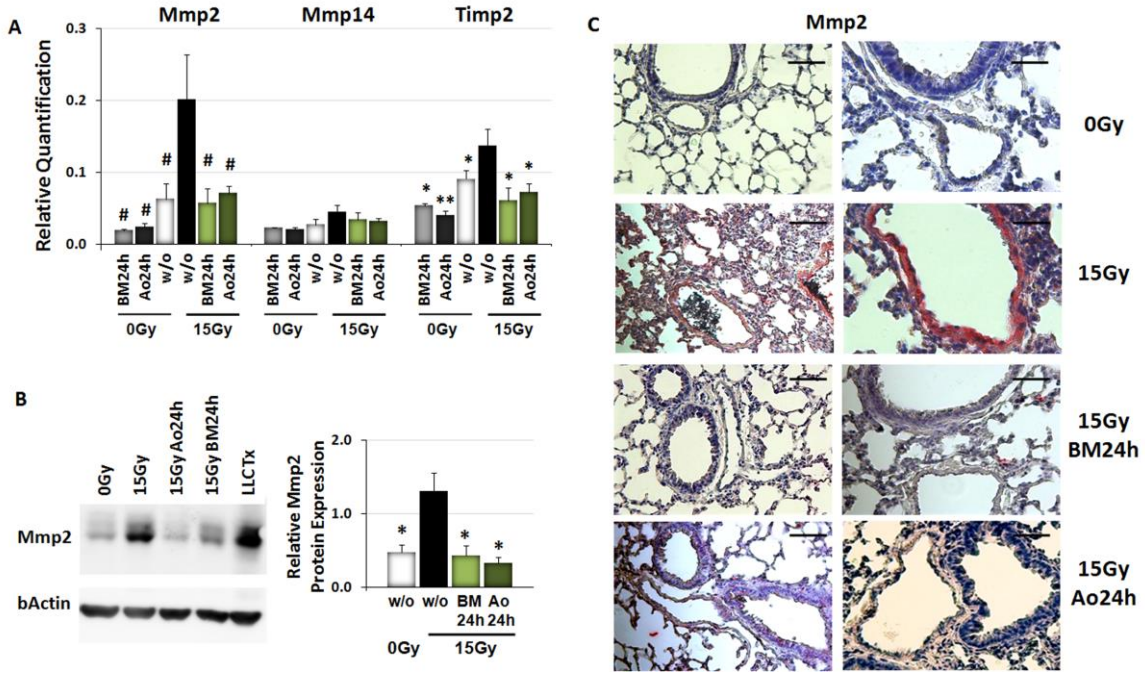

Figure 4

MSC treatment inhibits radiation-induced endothelial Mmp2 expression

C57BL/6 mice were left untreated or received a 15Gy WTI and were subsequently transplanted with cultured Ao or BM MSCs (0.5*10(6) cells) 24 hours after irradiation as indicated. (**A**) Real-Time RT-PCR quantification of the metastasis associated genes *matrix metalloproteinase 2* (*Mmp2*) as well as its activator Mmp14 and the co-factor *tissue inhibitor of metalloproteinases 2* (*Timp2*) in total lung RNA isolates derived 21 days after irradiation from control as well as WTI animals with or without subsequent MSC-therapy. Expression levels were normalized to the reference gene (beta Actin) and are shown as relative quantification. P values were indicated: *P<0.05, **P<0.01, #P<0.001 as analyzed by two-way ANOVA followed by post-hoc Bonferroni test (comparison to 15Gy). (**B**) Mmp2 expression was further analyzed in whole protein lysates using Western blot analysis. Representative blots from four different experiments are shown. Protein lysate from subcutaneously grown tumors of Lewis lung carcinoma cells (LLCTx) were included as positive control. For quantification blots were analyzed by densitometry and the Mmp2 signal was related to beta-actin. P-values were indicated: *$P \leq 0.05$, by one-way ANOVA followed by post-hoc Bonferroni test (comparison to 15Gy). (**C**) Lungs were dissected 21 days after

WTI and subjected to IHC analysis. Vessels were stained for Mmp2 using alkaline phosphatase staining (red). Nuclei were counterstained with Hemalaun (blue). Representative lung photographs from five different mice are shown. Scale bar = 25 µm, magnification scale bar = 10µm. “(To see this illustration in color the reader is referred to the web version of this article at www.liebertonline.com/ars)”

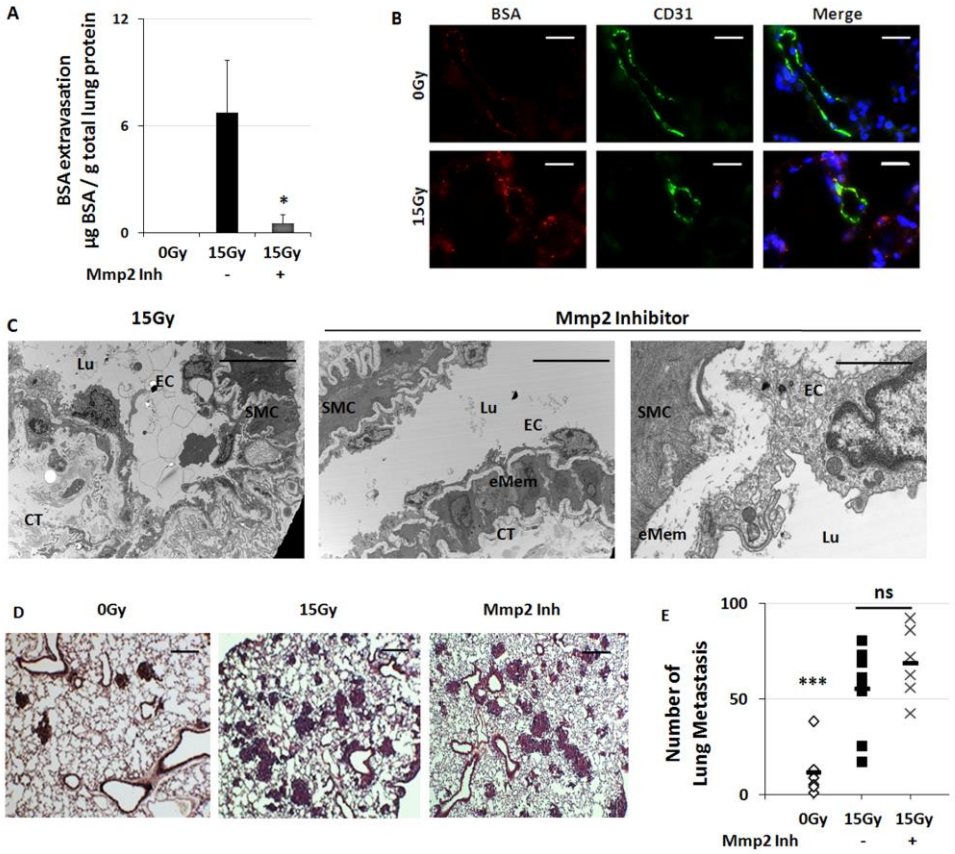

Figure 5

Mmp2 inhibition normalizes vascular function and but does not significantly alter WTI-induced seeding of circulating tumor cells

C57BL/6 mice received a WTI with 15Gy and were subsequently left untreated or received intraperitoneal injections of the selective Mmp2 inhibitor ARP100 (Mmp2 Inh; 15µg/g bodyweight) twice a week for 3 weeks post-irradiation. (**A**) Vascular leakage was determined at day 21 post-WTI by measuring extravasation of intravenously injected Alexa555-BSA to the lung interstitium 2-4h prior to the end of the experiment. Therefore 50µg BSA was intravenously injected into the tail vein prior sacrifice of mice by transcardial perfusion. Levels of extravasated Alexa555-BSA were determined in total cell lysates by measuring fluorescence intensity/ mg lysate. Data show means ± SEM (n = 4); $*P \leq 0.05$, by one-way ANOVA followed by post-hoc Bonferroni test. (**B)** Vascular leakage was further visualized by fluorescence-labeled BSA extravasation from the blood stream to the lung interstitium by immunofluorescence analysis. Tissue sections were stained for endothelial cells (CD31,

green). Fluorescence-labeled BSA is shown in red. Scale bar = 25 µm. (**C**) Morphological analysis of lung blood vessels was done using electron microscopy. Representative electron microscopy pictures of lung tissue from mice exposed to 15Gy WTI alone or the 15Gy WTI plus Mmp2 inhibitor as indicated are shown. SMC smooth muscle cell, eMem elastic membrane, Lu lumen, CT connective tissue. Scale bar: left and middle photograph = 10 µm, right photograph = 2µm. **(D)** Seeding and metastasis of circulating tumor cells to the lungs was analyzed 21 days after irradiation by intravenous injection of 1*10(6) B16F10 cells into the tail vein in mice exposed to 0Gy (sham control), 15Gy, or 15Gy WTI plus Mmp2 inhibitor treatment, respectively. 14d after tumor cell injection animals were sacrificed and lungs were isolated for quantification of lung metastases in whole lung sections after hematoxylin staining. (n=5 mice per group). Data show representative pictures of hematoxylin-stained lung sections. Scale bar = 100 µm. (**E**) Data show quantification of metastasis counts per lung section. Symbols depict separate mice; small black lines indicate means; numbers in the graph indicate P-values ***$P \leq 0.001$ (comparison to 15Gy) by one-way ANOVA followed by post-hoc Bonferroni test. The difference in mean counts of WTI mice and Mmp2 inhibitor-treated WTI mice (n = 6) is not significant. “(To see this illustration in color the reader is referred to the web version of this article at www.liebertonline.com/ars)”

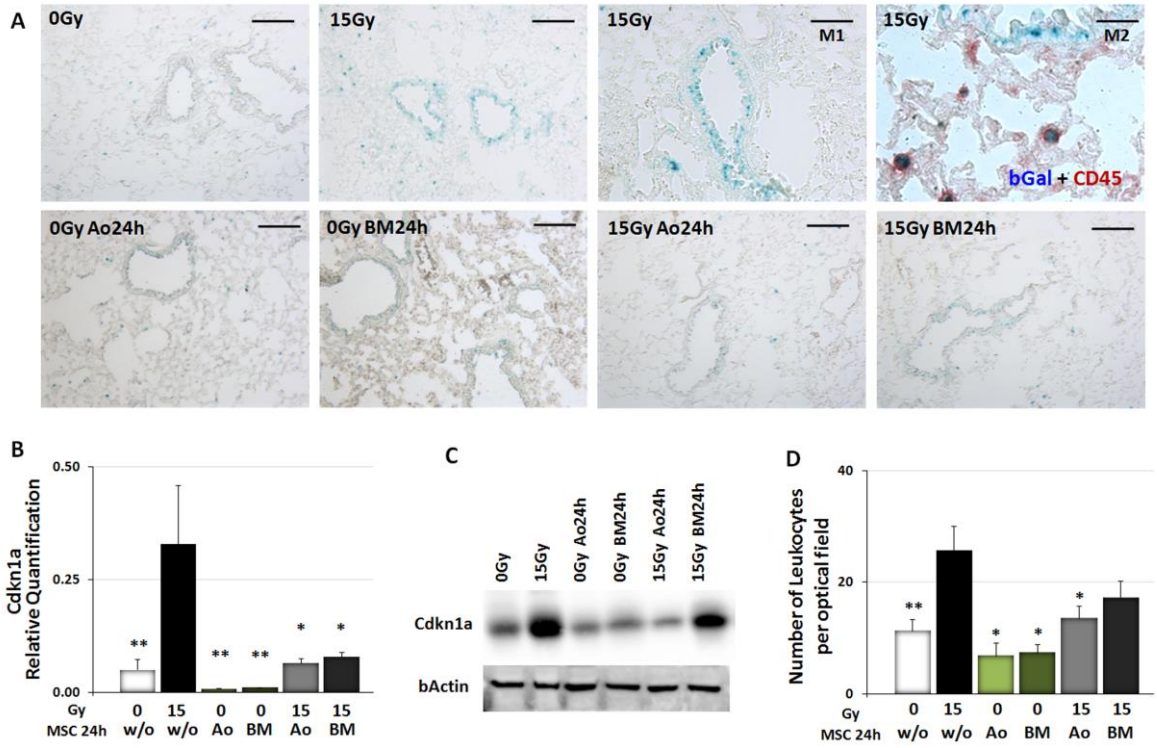

Figure 6

MSC treatment counteracts radiation-induced senescence of bronchial-alveolar epithelial cells

C57BL/6 mice were left untreated or received a 15Gy WTI and were subsequently transplanted with cultured Ao or BM MSCs (0.5*10(6) cells) 24 hours after irradiation as indicated. (**A**) Senescence-associated beta-galactosidase activity was assessed using frozen sections of lung tissue at 21 days after irradiation. Photomicrographs depict representative pictures of three independent experiments. Scale bar = 100 µm, M1 = 50µm, M2 = 10µm). (**B**) Real-Time RT-PCR quantification of the cellular senescence mediator gene *cyclin-dependent kinase inhibitor 1* (*Cdkn1a, p21*) was done using total lung RNA isolates. (**C**) Cdkn1a expression was further analyzed in whole lung protein lysates using Western blot analysis. Representative blots from three different experiments are shown. (**D**) Infiltrating CD45+ leukocytes were quantified by counting numbers of specific CD45-positive immunoreactive structures in four randomly chosen optical fields. Data are presented as mean ± SEM from four independent experiments. P-values were indicated: *$P \leq 0.05$, **$P < 0.01$ by two-way ANOVA (**B,D**) followed by post-hoc Bonferroni test (comparison to 15Gy).

"(To see this illustration in color the reader is referred to the web version of this article at www.liebertonline.com/ars)"

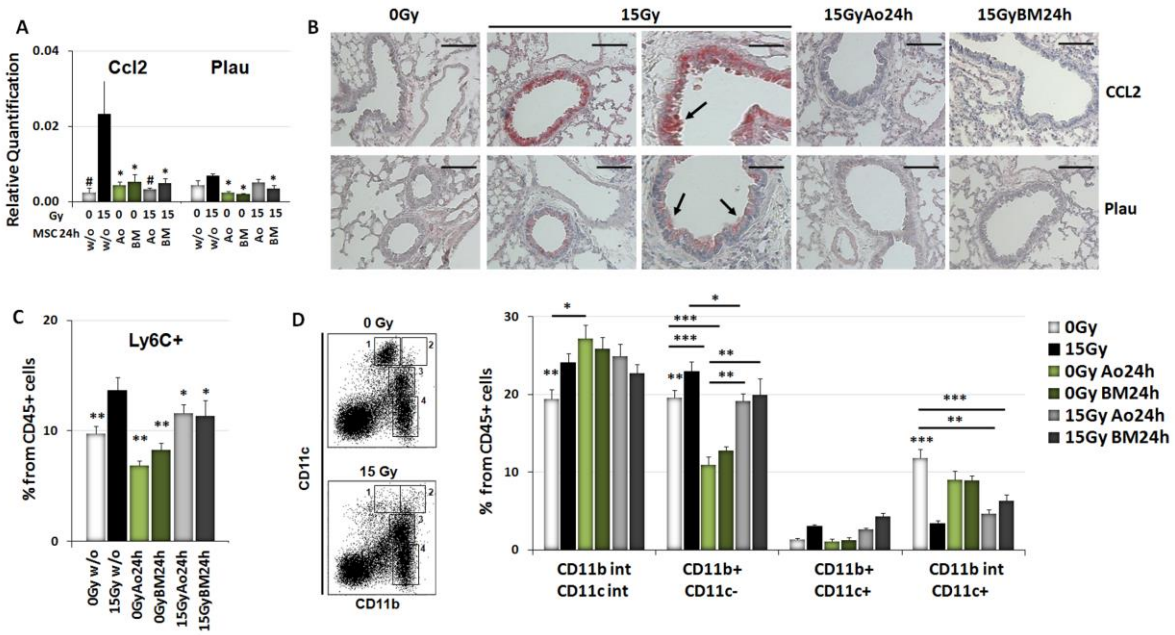

Figure 7

Radiation-induced expression of SASP factors is accompanied by an increased recruitment of inflammatory myeloid cells.

C57BL/6 mice were left untreated or received a 15Gy WTI and were subsequently transplanted with cultured Ao or BM MSCs (0.5*10(6) cells) 24 hours after irradiation as indicated. Lungs were collected at 21 days post-irradiation for further analysis. (**A**) Real-Time RT-PCR quantification of the SASP factors *urokinase-type plasminogen activator* (*uPA/ Plau*) and *chemokine (C-C motif) ligand 2* (*Ccl2*) was done using total lung RNA isolates. P values were indicated: *P<0.05, #P<0.001 as analyzed by two-way ANOVA followed by post-hoc Bonferroni test. (**B**) Immunohistochemical analysis of Ccl2 (upper panel) and Plau (lower panel) expression using alkaline phosphatase staining (red). Nuclei were counterstained with Hemalaun (blue). Representative lung photomicrographs of four different mice are shown. (Scale bar = 100 µm; magnification of 15Gy photographs scale bar = 40 µm). (**C+D**) Leukocytes in crude cell extracts of freshly isolated lung tissue were identified using CD45 expression and FACS analysis. Myeloid cells were further characterized using Ly6C (**C)** and CD11b, CD11c (**D**) antibodies. The gating strategy is shown in dotplots (D left panel): CD45+ leukocytes were gated from total lung cells and were further analyzed against CD11b and

CD11c. CD11b+ cells were sub-classified into high CD11b expressing cells (designated as "CD11b+ cells") and intermediate CD11b expressing cells (designated as "CD11b int cells"). CD45+ CD11b int/ CD11c int (gate 3) were designated as monocytes/ macrophages, CD11b+/ CD11c- (gate 4) as granulocytes/monocytes/neutrophils, CD11b+/ CD11c+ (gate 2) as macrophages/dendritic cells, and CD11b int/CD11c+ (gate 1) as alveolar macrophages. Data are presented as mean ± SEM from five independent experiments (0GyAo24h: n = 4; 0GyBM24h: n = 4; 0Gy: n = 15; 15Gy: n = 15; 15GyAo24h: n = 12; 15GyBM24h: n = 9). P-values were indicated: **P* ≤ 0.05, ***P* ≤ 0.01, ****P* ≤ 0.001 as analyzed by two-way ANOVA followed by post-hoc Bonferroni test [for **C**: F-factors 0.48 (interaction), 11.77 (cf / Gy), 1.268 (rf / treatment); for **D**: F-factors 9.026 (interaction), 1.025 (cf / Gy), 327.5(rf / marker)]. "(To see this illustration in color the reader is referred to the web version of this article at www.liebertonline.com/ars)"

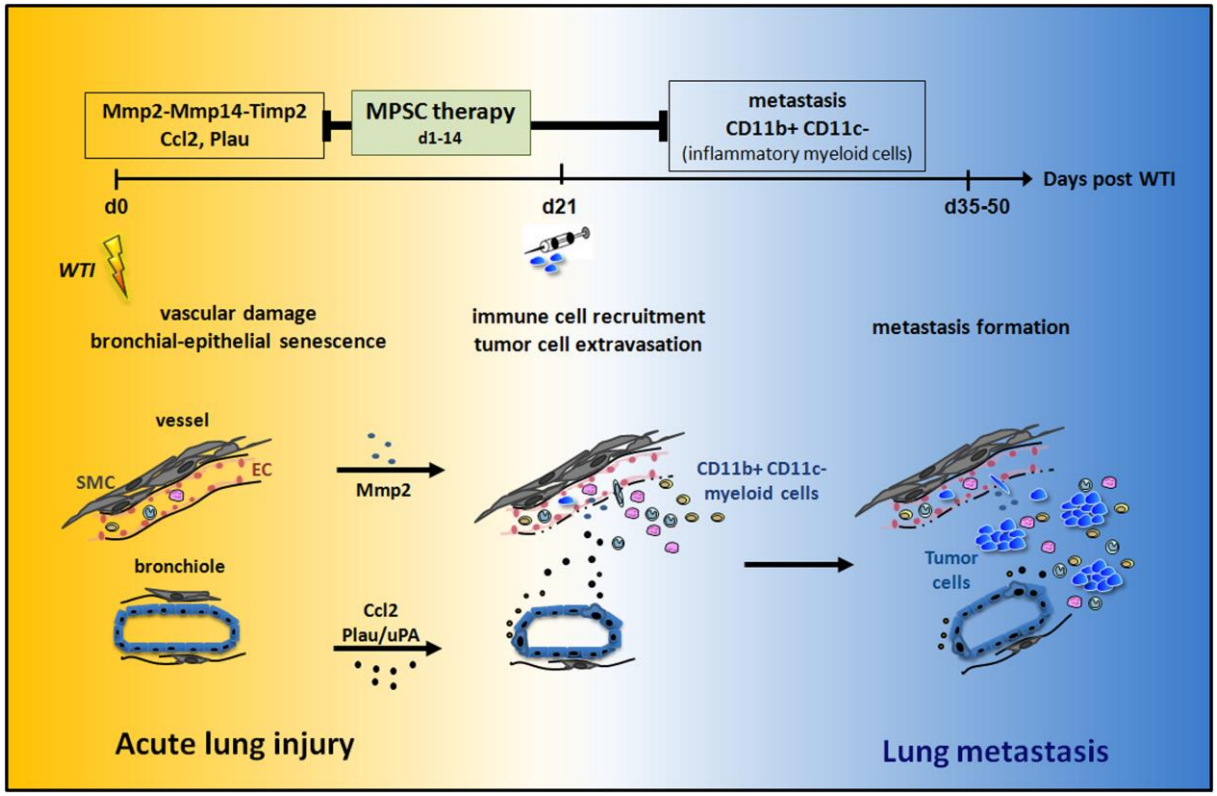

Figure 8

MSC-therapy counteracts a tumor-promoting paracrine network initiated by radiation-induced damage to resident cells

Though the reason for the formation of micrometastasis in specific organs is still unknown, this process requires adhesion of the tumor cells to the vessel wall and subsequent emigration into the surrounding tissue. Normal lung capillaries provide an efficient barrier to tumor cell extravasation. WTI considerably enhanced tumor cell extravasation and lung metastasis. Pro-invasive cellular activities were accompanied by radiation-induced endothelial cell damage and up-regulation of the Mmp2-Mmp14-Timp2 axis as well as increased senescence-associated secretory phenotype (SASP) factor production (Plau/uPA, Ccl2) by senescent bronchial-alveolar epithelial cells. In addition, an increased number of immune cells were recruited to previously irradiated lung tissue; in particular the number of CD11b+CD11c- myeloid cells was significantly increased after radiation therapy. The pro-metastatic radiation effect was blocked by treating mice with cultured multipotent mesenchymal stromal cells (MSCs) derived either from bone marrow (BM) or from aorta (Ao)

within the first 2 weeks after irradiation. This study provides novel insight into the mechanisms of radiation-induced tumor-promoting effects and potential protective strategies.

"(To see this illustration in color the reader is referred to the web version of this article at www.liebertonline.com/ars)"